IO
Long Waves and
Ocean Tides

Myrl C. Hendershott

10.1 Introduction

The main purpose of this chapter is to summarize what was generally known to oceanographers about long waves and ocean tides around 1940, and then to indicate how the subject has developed since then, with particular emphasis upon those aspects that have had significance for oceanography beyond their importance in understanding tides themselves. I have begun with a description of astronomical and radiational tide-generating potentials (section 10.2), but say no more than is necessary to make this chapter self-contained. Cartwright (1977) summarizes and documents recent developments, and I have followed his discussion closely.

The fundamental dynamic equations governing tides and long waves, Laplace's tidal equations (LTE), remained unchanged and unchallenged from Laplace's formulation of them in 1776 up to the early twentieth century. By 1940 they had been extended to allow for density stratification (in the absence of bottom relief) and criticized for their exclusion of half of the Coriolis forces. Without bottom relief this exclusion has recently been shown to be a good approximation; the demonstration unexpectedly requires the strong stratification of the ocean. Bottom relief appears able to make long waves in stratified oceans very different from their flat-bottom counterparts (section 10.4); a definitive discussion has not yet been provided. Finally, LTE have had to be extended to allow for the gravitational self-attraction of the oceans and for effects due to the tidal yielding of the solid earth. I review these matters in section 10.3.

Laplace's study of the free oscillations of a global ocean governed by LTE was the first study of oceanic long waves. Subsequent nineteenth- and twentieth-century explorations of the many free waves allowed by these equations, extended to include stratification, have evolved into an indispensible part of geophysical fluid dynamics. By 1940, most of the flat-bottom solutions now known had, at least in principle, been constructed. But Rossby's rediscovery and physical interpretation, in 1939, of Hough's oscillations of the second class began the modern period of studying solutions of the long-wave equations by inspired or systematic approximation and of seeking to relate the results to nontidal as well as tidal motions. Since then, flat-bottom barotropic and baroclinic solutions of LTE have been obtained in mid-latitude and in equatorial approximation, and Laplace's original global problem has been completely solved. The effects of bottom relief on barotropic motion are well understood. Significant progress has been made in understanding the effects of bottom relief on baroclinic motions. I have attempted to review all those developments in a self-contained manner in section 10.4. In order to treat this

vast subject coherently, I have had to impose my own view of its development upon the discussion. I have cited observations when they appear to illustrate some property of the less familiar solutions, but the central theme is a description of the properties of theoretically possible waves of long period (greater than the buoyancy period) and, consequently, of length greater than the ocean's mean depth.

Although the study of ocean surface tides was *the* original study of oceanic response to time-dependent forcing, tidal studies have largely proceeded in isolation from modern developments in oceanography on account of the strength of the tide-generating forces, their well-defined discrete frequencies, and the proximity of these to the angular frequency of the earth's rotation. A proper historical discussion of the subject, although of great intellectual interest, is beyond the scope of this chapter. To my mind the elements of such a discussion, probably reasonably complete through the first decade of this century, are given in Darwin's 1911 *Encyclopedia Britannica* article "Tides." Thereafter, with a few notable exceptions, real progress had to await modern computational techniques both for solving LTE and for making more complete use of tide gauge observations. Cartwright (1977) has recently reviewed the entire subject, and therefore I have given a discussion in section 10.5 that, although self-contained, emphasizes primarily changes of motivation and viewpoint in tidal studies rather than recapitulates Cartwright's or other recent reviews.

This discussion of tides as long waves continuously forced by lunar and solar gravitation logically could be followed by a discussion of tsunamis impulsively forced by submarine earthquakes. But lack of both space and time has forced omission of this topic.

Internal tides were first reported at the beginning of this century. By 1940 a theoretical framework for their discussion had been supplied by the extension of LTE to include stratification, and their generation was (probably properly) ascribed to scattering of barotropic tidal energy from bottom relief. The important developments since then are recognition of the intermittent narrow-band nature of internal tides (as opposed to the near-line spectrum of surface tides) plus the beginnings of a statistically reliable characterization of the internal tidal spectrum and its variation in space and time. The subject has recently been reviewed by Wunsch (1975). Motivation for studying internal tides has shifted from the need for an adequate description of them through exploration of their role in global tidal dissipation (now believed to be under 10%) to speculation about their importance as energy sources for oceanic mixing. In section 10.6 I have summarized modern observational studies and their implications for tidal mixing of the oceans.

Many features of the presentday view of ocean circulation have some precedent in tidal and long-wave studies, although often unacknowledged and apparently not always recognized. The question of which parts of the study of tides have in fact influenced the subsequent development of studies of ocean circulation is a question for the history of science. In some cases, developments in the study of ocean circulation subsequently have been applied to ocean tides. In section 10.7 I have pointed out some of the connections of which I am aware.

10.2 Astronomical Tide-Generating Forces

Although correlations between ocean tides and the position and phase of the moon have been recognized and utilized since ancient times, the astronomical tide-generating force (ATGF) was first explained by Newton in the *Principia* in 1687. Viewed in an accelerated coordinate frame that moves with the center of the earth but that does not rotate with respect to the fixed stars, the lunar (solar) ATGF at any point on the earth's surface is the difference between lunar (solar) gravitational attraction at that point and at the earth's center. The daily rotation of the earth about its axis carries a terrestrial observer successively through the longitude of the sublunar or subsolar point [at which the lunar (solar) ATGF is toward the moon (sun)] and then half a day later through the longitude of the antipodal point [at which the ATGF is away from the moon (sun)]. In Newton's words, "It appears that the waters of the sea ought twice to rise and twice to fall every day, as well lunar or solar" [Newton, 1687, proposition 24, theorem 19].

The ATGF is thus predominantly semidiurnal with respect to both the solar and the lunar day. But it is not entirely so. Because the tide-generating bodies are not always in the earth's equatorial plane, the terrestrial observer [who does not change latitude while being carried through the longitude of the sublunar (solar) point or its antipode] sees a difference in amplitude between the successive semidiurnal maxima of the ATGF at his location. This difference or "daily inequality" means that the ATGF must be thought of as having diurnal as well as semidiurnal time variation.

Longer-period variations are associated with periodicities in the orbital motion of earth and moon. The astronomical variables displaying these long-period variations appear nonlinearly in the ATGF. The long-period orbital variations thus interact nonlinearly both with themselves and with the short-period diurnal and semidiurnal variation of the ATGF to make the local ATGF a sum of three narrow-band processes centered about 0, 1, and 2 cycles per day (cpd), each process being a sum of motions harmonic at multiples 0,1,2 of the frequencies corresponding to a lunar or a solar day

plus sums of multiples of the frequencies of long-period orbital variations.

A complete derivation of the ATGF is beyond the scope of this discussion. Cartwright (1977) reviews the subject and supplies references documenting its modern development. For a discussion that concentrates upon ocean dynamics (but not necessarily for a practical tide prediction), the most convenient representation of the ATGF is as a harmonic decomposition of the tide-generating potential whose spatial gradient is the ATGF. Because only the horizontal components of the ATGF are of dynamic importance, it is convenient to represent the tide-generating potential by its horizontal and time variation U over some near-sea-level equipotential (the geoid) of the gravitational potential due to the earth's shape, internal mass distribution, and rotation. To derive the dynamically significant part of the ATGF it suffices to assume this surface spherical. U/g (where g is the local gravitational constant, unchanging over the geoid) has the units of sea-surface elevation and is called the *equilibrium tide* $\bar{\zeta}$. Its principle term is (Cartwright, 1977)

$$\bar{\zeta}(\phi,\theta,t) = U(\phi,\theta,t)/g$$

$$= \sum_{m=0,1,2} (A_2^m \cos m\phi + B_2^m \sin m\phi)P_2^m, \qquad (10.1)$$

in which ϕ,θ are longitude and latitude, the $P_2^m(\theta)$ are associated Legendre functions

$$P_2^0 = \tfrac{1}{2}(3\cos^2\bar{\theta} - 1),$$

$$P_2^1 = 3\sin\bar{\theta}\cos\bar{\theta}, \qquad (10.2)$$

$$P_2^2 = 3\sin^2\bar{\theta}$$

of colatitude $\bar{\theta} = (\pi/2) - \theta$, and A_2^m, B_2^m are functions of time having the form

$$A_n^m(t) = \sum_i M_i {\cos \atop \sin} \left[\sum_{j=1}^{6} N_j^{(i)}S_j(t) \right]. \qquad (10.3)$$

The M_i are amplitudes obtained from Fourier analysis of the astronomically derived time series $U(\phi,\theta,t)/g$;

the $N_j^{(i)}$ are sets of small integers (effectively the Doodson numbers); and the $S_j(t)$ are secular arguments that increase almost linearly in time with the associated periodicity of a lunar day, a sidereal month, a tropical year, 8.847 yr (period of lunar perigee), 18.61 yr (period of lunar node), 2.1 × 10⁴ yr (period of perihelion), respectively.

The frequencies of the arguments $\Sigma N_j^{(i)}S_j(t)$ fall into the three "species"—long period, diurnal, and semidiurnal—which are centered, respectively, about 0, 1, and 2 cpd ($N_1 = 0,1,2$). Each species is split into "groups" separated by about 1 cycle per month, groups are split into "constituents" separated by one cyle per year, etc. Table 10.1 lists selected constituents. In the following discussion they are referred to by their Darwin symbol (see table 10.1).

An important development in modern tidal theory has been the recognition that the ATGF is not the only important tide-generating force. Relative to the amplitudes and phases of corresponding constituents of the equilibrium tide, solar semidiurnal, diurnal, and annual ocean tides usually have amplitudes and phases quite different from the amplitudes and phases of other nearby constituents. Munk and Cartwright (1966) attributed these anomalies in a general way to solar heating and included them in a generalized equilibrium tide by defining an ad hoc radiational potential (Cartwright, 1977)

$$U_R(\phi,\theta,t) = \begin{cases} S(\xi/\bar{\xi})\cos\alpha, & 0 < \alpha < \pi/2: \\ 0, & \pi/2 < \alpha < \pi: \end{cases} \qquad (10.4)$$

which is zero at night, which varies as the cosine of the sun's zenith angle α during the day, and which is proportional to the solar constant S and the sun's parallax ξ (mean $\bar{\xi}$). Cartwright (1977) suggests that for the oceanic S_2 (principal solar) tide, whose anomalous portion is about 17% of the gravitational tide (Zetler, 1971), the dominant nongravitational driving is by the atmospheric S_2 tide. Without entering further into the discussion, I want to point out that the global form of

Table 10.1 Characteristics of Selected Constituents of the Equilibrium Tide

Darwin symbol	N_1, N_2, N_3, N_4				Period (solar days or hours)	Amplitude M (m)	Spatial variation
S_{sa}	0	0	2	0	182.621 d	0.02936	
M_m	0	1	0	-1	27.55 d	0.03227	$\tfrac{1}{2}(3\cos^2\bar{\theta} - 1)$
M_f	0	2	0	0	13.661 d	0.0630	
O_1	1	-1	0	0	25.82 h	0.06752	
P_1	1	1	-2	0	24.07 h	0.03142	$3\sin\bar{\theta}\cos\bar{\theta} \times \sin(\omega_1 t + \phi)$
K_1	1	1	0	0	23.93 h	0.09497	
N_2	2	-1	0	1	12.66 h	0.01558	
M_2	2	0	0	0	12.42 h	0.08136	$3\sin^2\bar{\theta} \times \cos(\omega_2 t + 2\phi)$
S_2	2	2	-2	0	12.00 h	0.03785	
K_2	2	2	0	0	11.97 h	0.01030	

Myrl C. Hendershott

the atmospheric S_2 tide is well known (Chapman and Lindzen, 1970), so that the same numerical programs that have been used to solve for global gravitationally driven ocean tides could easily be extended to allow for atmospheric-pressure driving of the oceanic S_2 tide.

Ocean gravitational self-attraction and tidal solid-earth deformation are quantitatively even more important in formulating the total tide-generating force than are thermal and atmospheric effects. They are discussed in the following section, since they bring about a change in the form of the dynamic equations governing ocean tides.

10.3 Laplace's Tidal Equations (LTE) and the Long-Wave Equations

Laplace (1775, 1776; Lamb, 1932, §213–221) cast the dynamic theory of tides essentially in its modern form. His tidal equations (LTE) are usually formally obtained from the continuum equations of momentum and mass conservation (written in rotating coordinates for a fluid shell surrounding a nearly spherical planet and having a gravitationally stabilized free surface) by assuming (Miles, 1974a)

(1) a perfect homogeneous fluid,
(2) small disturbances relative to a state of uniform rotation,
(3) a spherical earth,
(4) a geocentric gravitational field uniform horizontally and in time,
(5) a rigid ocean bottom,
(6) a shallow ocean in which both the Coriolis acceleration associated with the horizontal component of the earth's rotation and the vertical component of the particle acceleration are neglected.

The resulting equations are

$$\frac{\partial u}{\partial t} - 2\Omega \sin\theta v = -\frac{\partial}{\partial\phi}(\zeta - \Gamma/g)/a \cos\theta, \qquad (10.5a)$$

$$\frac{\partial v}{\partial t} + 2\Omega \sin\theta u = -\frac{\partial}{\partial\theta}(\zeta - \Gamma/g)/a, \qquad (10.5b)$$

$$\frac{\partial\zeta}{\partial t} + \frac{1}{a\cos\theta}\left[\frac{\partial}{\partial\phi}(uD) + \frac{\partial}{\partial\theta}(vD\cos\theta)\right] = 0. \qquad (10.5c)$$

In these, (ϕ, θ) are longitude and latitude with corresponding velocity components (u, v), ζ the ocean surface elevation, Γ the tide-generating potential, $D(\phi, \theta)$ the variable depth of the ocean, a the earth's spherical radius, g the constant gravitational attraction at the earth's surface, and Ω the earth's angular rate of rotation.

Two modern developments deserve discussion. They are a quanitative formulation and study of the mathematical limit process implicit in assumptions (1) through (6), and the realization that assumptions (4)

and (5) are quantitatively inadequate for a dynamic discussion of ocean tides.

It has evidently been recognized since the work of Bjerknes, Bjerknes, Solberg, and Bergeron (1933) that assumption (6) (especially the neglect of Coriolis forces due to the horizontal component of the earth's rotation) amounts to more than a minor perturbation of the spectrum of free oscillations that may occur in a thin homogeneous ocean. Thus Stern (1963) and Israeli (1972) found axisymmetric equatorially trapped normal modes of a rotating spherical shell of homogeneous fluid that are extinguished by the hydrostatic approximation. Indeed, Stewartson and Rickard (1969) point out that the limiting case of a vanishingly thin homogeneous ocean is a nonuniform limit: the solutions obtained by solving the equations and then taking the limit may be very different from those obtained by first taking the limit and then solving the resulting approximate (LTE) equations. Quite remarkably, it is the reinstatement of realistically large stratification, i.e., the relaxation of assumption (1), that saves LTE as an approximate set of equations whose solutions are uniformly valid approximations to some of the solutions of the full equations when the ocean is very thin.

The parodoxical importance of stratification for the validity of the ostensibly unstratified LTE appears to have been recognized by Proudman (1948) and by Bretherton (1964). Phillips (1968) pointed out its importance at the conclusion of a correspondence with Veronis (1968b) concerning the effects of the "traditional" approximation (Eckart, 1960; N. A. Phillips, 1966b), i.e., the omission of the Coriolis terms $2\Omega \cos\theta w$ and $-2\Omega \cos\theta u$, in (10.6)–(10.8) below. But it was first explicitly incorporated into the limit process producing LTE by Miles (1974a) who addressed all of assumptions (1) through (6) by defining appropriate small parameters and examining the properties of expansions in them. He found that the simplest set of uniformly valid equations for what I regard as long waves in this review are

$$\frac{\partial u}{\partial t} - 2\Omega \sin\theta v + 2\Omega \cos\theta w = -\frac{\partial p}{\partial\phi}\frac{1}{\bar\rho_0 a \cos\theta}, \qquad (10.6a)$$

$$\frac{\partial v}{\partial t} + 2\Omega \sin\theta u = -\frac{\partial p}{\partial\theta}\frac{1}{\bar\rho_0 a}, \qquad (10.6b)$$

$$N^2 w - 2\Omega \cos\theta \frac{\partial u}{\partial t} = -\frac{\partial^2\rho}{\partial z \,\partial t}\frac{1}{\bar\rho_0}, \qquad (10.6c)$$

$$\frac{\partial u}{\partial\phi} + \frac{\partial(v\cos\theta)}{\partial\theta} + a\cos\theta \frac{\partial w}{\partial z} = 0, \qquad (10.6d)$$

with boundary conditions

$$w = 0 \quad \text{at} \quad z = -D_*$$

(for uniform depth D_*), $\qquad\qquad\qquad (10.7)$

$$p = -\bar{\rho}_0 g \zeta_0 \quad \text{at} \quad z = 0. \tag{10.8}$$

In these, z is the upward local vertical with associated velocity component w, p the deviation of the pressure from a resting hydrostatic state characterized by the stable density distribution $\rho_0(z)$, $\bar{\rho}_0$ a constant characterizing the mean density of the fluid (the Boussinesq approximation has been made in its introduction); the buoyancy frequency

$$N(z) = \left(-\frac{g}{\rho_0} \frac{\partial \rho_0}{\partial z} - \frac{g^2}{c^2} \right)^{1/2} \tag{10.9}$$

is the only term in which allowance for compressibility (c is the local sound speed) is important in the ocean.

Miles (1974a) further found that when $N^2(z) \gg 4\Omega^2$, free solutions of LTE for a uniform-depth (D_*) ocean covering the globe also solve (10.6)–(10.8) with an error which is of order $(\sigma/2\Omega)(4\Omega^2 a/g) \ll 1$, where σ is the frequency of oscillation of the free solutions. LTE surface elevations ζ are consequently in error by order $(D_*/a)(D_* N^2/g)^{-3/4}$, while LTE velocities u,v may be in error by $(D_*/a)(D_* N^2/g)^{-1/4}$. Miles (1974a) obtained this result by taking the (necessarily barotropic) solutions of LTE as the first term of an expansion of the solutions of (10.6)–(10.8) in the parameter $(\sigma/2\Omega)(4\Omega^2 a/g)$, which turns out to characterize the relative importance of terms neglected and terms retained in making assumption (6). The next term in the expansion consists of internal wave modes (see section 10.4.3). Because their free surface displacements are very small relative to internal displacements, the overall free surface displacement remains as in LTE although in the interior of the ocean, internal wave displacements and currents may well dominate the motion.

The analysis is inconclusive at frequencies or depths at which the terms assumed to be correction perturbations are resonant. Finding expressions for all the free oscillations allowed by Miles's simplest uniformly valid system (10.6)–(10.8) involves as yet unresolved mathematical difficulties associated with the fact that these equations are hyperbolic over part of the spatial domain when the motion is harmonic in time (Miles, 1974a).

Application of this analysis to ocean tides is further circumscribed by its necessary restriction to a global ocean of constant depth. I speculate that if oceanic internal modes are sufficiently inefficient as energy transporters that they cannot greatly alter the energetics of the barotropic solution unless their amplitudes are resonantly increased beyond observed levels (section 10.6), and if they are sufficiently dissipative that they effectively never are resonant, then an extension of this analysis to realistic basins and relief would probably confirm LTE as adequate governors of the surface elevation. The ideas, necessary for such an

extension, that is, how variable relief and stratification influence barotropic and baroclinic modes, are beginning to be developed (see section 10.4.7).

Miles (1974a) discusses assumptions (3)–(5) with explicit omission of ocean gravitational self-attraction and solid-earth deformation. Self-attraction was included in Hough's (1897, 1898; Lamb, 1932, §222–223) global solutions of LTE. Thomson (1863) evidently first pointed out the necessity of allowing for solid-earth deformation. Both are quantitatively important. The latter manifests itself in a geocentric solid-earth tide δ plus various perturbations of the total tide-generating potential Γ. Horizontal pressure gradients in LTE (10.5) are associated with gradients of the geocentric ocean tide ζ, but it is the observed ocean tide

$$\zeta_0 = \zeta - \delta \tag{10.10}$$

that must appear in the continuity equation of (10.5c).

All these effects are most easily discussed (although not optimally computed) when the astronomical potential U, the observed ocean tide ζ_0, the solid earth tide δ, and the total tide-generating potential Γ are all decomposed into spherical harmonic components U_n, ζ_{0n}, δ_n, and Γ_n. The Love numbers k_n, h_n, k_n', h_n', which carry with them information about the radial structure of the solid earth (Munk and McDonald, 1960), and the parameter $\alpha_n = (3/2n + 1)(\bar{\rho}_{ocean}/\bar{\rho}_{earth})$ then appear naturally in the development. The total tide-generating potential Γ_n contains an astronomical contribution U_n (primarily of order $n = 2$), an augmentation $k_n U_n$ of this due to solid earth yielding to $-\nabla U_n$, an ocean self-attraction contribution $g\alpha_n\zeta_{0n}$, and a contribution $k_n' g\alpha_n\zeta_{0n}$ due to solid-earth deformation by ocean self-attraction and tidal column weight. Thus

$$\Gamma_n = (1 + k_n)U_n + (1 + k_n')g\alpha_n\zeta_{0n}. \tag{10.11}$$

There is simultaneously a geocentric solid-earth tide δ made up of the direct yielding $h_n U_n g$ of the solid earth to $-\nabla U_n$ plus the deformation $h_n' g\alpha_n\zeta_{0n}$ of the solid earth by ocean attraction and tidal column weight. Thus

$$\delta_n = h_n U_n/g + h_n' g\alpha_n\zeta_{0n}. \tag{10.12}$$

For computation, Farrell (1972a) has constructed a Green's function such that

$$\sum_n (1 + k_n' - h_n')\alpha_n\zeta_{0n}$$

$$= \iint_{\text{ocean}} d\theta' \, d\phi' \cos\theta' \, G(\phi',\theta'|\phi,\theta)\zeta_0(\phi',\theta'). \tag{10.13}$$

With $U_n = U_2$ and with (10.13) abbreviated as $\iint G\zeta_0$, LTE with assumptions (4) and (5) appropriately relaxed become

Myrl C. Hendershott

$$\frac{\partial u}{\partial t} - 2\Omega \sin\theta\, v = -\frac{g}{a\cos\theta}\frac{\partial}{\partial\phi}\,[\zeta_0 - (1 + k_2 - h_2)U_2/g$$

$$-\iint G\zeta_0], \qquad (10.14a)$$

$$\frac{\partial v}{\partial t} + 2\Omega \sin\theta\, u = -\frac{g}{a}\frac{\partial}{\partial\theta}\,[\zeta_0 - (1 + k_2 - h_2)U_2/g$$

$$-\iint G\zeta_0], \qquad (10.14b)$$

$$\frac{\partial\zeta_0}{\partial t} + \frac{1}{a\cos\theta}\left[\frac{\partial(uD)}{\partial\phi} + \frac{\partial(vD\cos\theta)}{\partial\theta}\right] = 0. \qquad (10.14c)$$

The factor $1 + k_2 - h_2 \simeq 0.69$ is clearly necessary for a quantitatively correct solution. The term $\iint G\zeta_0$ was first evaluated by Farrell (1972b). I wrote down (10.14) and attempted to estimate the effect of $\iint G\zeta_0$ on a global numerical solution of (10.14) for the M_2 tide by an iterative procedure which, however, failed to converge (Hendershott, 1972). Subsequent computations by Gordeev, Kagan, and Polyakov (1977) and by Accad and Pekeris (1978) provide improved estimates of the effects (see section 10.5.3).

With appropriate allowance for various dissipative processes (including all mechanisms that put energy into internal tides), I regard (10.14) as an adequate approximation for studying the ocean surface tide. Oceanic long waves should really be discussed using (10.6) but allowing for depth variations by putting

$$w = \mathbf{u} \cdot \nabla D \qquad \text{at} \quad z = -D(\phi, \theta) \qquad (10.15)$$

in place of (10.7). Miles (1974a) derives an orthogonality relationship that could be specialized to (10.6)–(10.8) in the case of constant depth, but even then the nonseparability of the eigenfunctions into functions of (ϕ, θ) times functions of z has prevented systematic study of the problem. Variable relief compounds the difficulty. Most studies either deal with surface waves over bottom relief, and thus start with LTE (10.5), or else with surface and internal waves over a flat bottom. In the latter case, (10.6)–(10.8) are solved but with the Coriolis terms $2\Omega \cos\theta\, w$ and $-2\Omega \cos\theta\, u$ arbitrarily neglected (the "traditional" approximation). Miles' (1974a) results appear to justify this procedure for the former case, but Munk and Phillips (1968) show that the neglected terms are proportional to (mode number)$^{1/3}$ for internal modes so that the traditional approximation may be untenable for high-mode internal waves. The following discussion (section 10.4) of oceanic long waves relies heavily upon the traditional approximation, but it is important to note that its domain of validity has not yet been entirely delineated.

10.4 Long Waves in the Ocean

10.4.1 Introduction

The first theoretical study of oceanic long waves is due to Laplace (1775, 1776; Lamb, 1932, §213–221), who solved LTE for an appropriately shallow ocean covering a rotating rigid spherical earth by expanding the solution in powers of $\sin\theta$. For a global ocean of constant depth D_*, Hough (1897, 1898; Lamb, 1932, §222–223) obtained solutions converging rapidly for small

$$\Lambda = 4\Omega^2 a^2/gD_* \qquad (10.16)$$

(sometimes called Lamb's parameter) by expanding the solution in spherical harmonics $P_n^l\,(\sin\theta)\exp(il\phi)$. He found the natural oscillations to be divided into first- and second-class modes whose frequencies σ are given, respectively, by

$$\sigma = \pm[n(n + 1)gD_*/a^2]^{1/2},$$

$$\sigma = -2\Omega l/[n(n + 1)] \qquad (10.17)$$

as $\Lambda \to 0$. But $\Lambda \simeq 20$ for $D_* = 4000$ m, and is very much larger for internal waves (see section 10.4.3). A correspondingly complete solution of Laplace's problem, valid for large as well as small Λ, was given only recently (Flattery, 1967; Longuet-Higgins, 1968a). Physical understanding of the solutions has historically been developed by studying simplified models of LTE.

10.4.2 Long Waves in Uniformly Rotating Flat-Bottomed Oceans

Lord Kelvin (Thomson, 1879; Lamb, 1932, §207) introduced the idealization of uniform rotation, at Ω, of a sheet of fluid about the vertical (z-axis). LTE become

$$\frac{\partial u}{\partial t} - f_0 v = -g\frac{\partial\zeta}{\partial x}, \qquad (10.18a)$$

$$\frac{\partial v}{\partial t} + f_0 u = -g\frac{\partial\zeta}{\partial y}, \qquad (10.18b)$$

$$\frac{\partial\zeta}{\partial t} + \frac{\partial(uD)}{\partial x} + \frac{\partial(vD)}{\partial y} = 0. \qquad (10.18c)$$

f_0, here equal to 2Ω, is the Coriolis parameter. Lord Kelvin's plane model (10.18) is often called the f-plane.

The solid earth is nearly a spheroid of equilibrium under the combined influence of gravity g and centrifugal acceleration $\Omega^2 a$; the earth's equatorial radius is about 20 km greater than its polar radius. Without water motion, the sea surface would have a congruent spheroidal shape. Taking the depth constant in LTE models this similarity; the remaining error incurred by working in spherical rather than spheroidal coordinates is (Miles, 1974a) of order $\Omega^2 a/g = 10^{-3}$. It is correspondingly appropriate to take the depth constant in Lord Kelvin's plane model (10.18) in order to obtain planar

solutions locally modeling those of LTE with constant depth. But the laboratory configuration corresponding to constant depth in (10.18c) is a container with a paraboloidal bottom $\frac{1}{2}\Omega^2(x^2 + y^2)/g$ rather than a flat bottom [see Miles (1964) for a more detailed analysis].

Without rotation ($f_0 = 0$) and with constant depth ($D = D_*$) Lord Kelvin's plane model reduces to the linearized shallow-water equations (LSWE). For an unbounded fluid sheet, they have plane gravity-wave solutions

$$\zeta = a \exp(-i\sigma t + ilx + iky), \tag{10.19a}$$

$$u = (gl/\sigma)\zeta, \tag{10.19b}$$

$$v = (gk/\sigma)\zeta, \tag{10.19c}$$

$$w = -i\sigma(z/D_* + 1)\zeta, \tag{10.19d}$$

$$\sigma^2 = gD_*(l^2 + k^2), \tag{10.19e}$$

which are dispersionless [all travel at $(gD_*)^{1/2}$] and are longitudinal [(u, v) parallel to (l, k)]. Horizontal particle accelerations are exactly balanced by horizontal pressure-gradient forces while vertical accelerations are negligible. Such waves reflect specularly at a straight coast with no phase shift; thus

$$\zeta = a \exp(-i\sigma t + ilx + iky)$$
$$+ a \exp(-i\sigma t - ilx + iky) \tag{10.20}$$

satisfies $u = 0$ at the coast $x = 0$, the angle $\tan^{-1}(k/l)$ of incidence equals the angle of reflection, and the (complex) reflected amplitude equals the incident amplitude a. The normal modes of a closed basin with perimeter P are the eigensolutions $Z_n(x,y)\exp(-i\sigma_n t)$, σ_n of

$$\nabla_2^2 Z_n + (\sigma_n^2/gD_*)Z_n = 0 \tag{10.21}$$

with

$$\partial Z_n/\partial(\text{normal}) = 0 \quad \text{on} \quad P. \tag{10.22}$$

If P is a constant surface in one of the coordinate systems in which ∇_2^2 separates, then the normal modes are mathematically separable functions of the two horizontal space coordinates and so are readily discussed in terms of appropriate special functions. Even in general basin shapes, the existence and completeness of the normal modes are assured (Morse and Feshbach, 1953).

With rotation, plane wave solutions of (10.18) with constant depth D_* are

$$\zeta = a \exp(-i\sigma t + ilx + iky), \tag{10.23a}$$

$$u = g[(l\sigma + ikf_0)/(\sigma^2 - f_0^2)]\zeta, \tag{10.23b}$$

$$v = g[(k\sigma - ilf_0)/(\sigma^2 - f_0^2)]\zeta, \tag{10.23c}$$

$$w = -i\sigma(z/D_* + 1)\zeta, \tag{10.23d}$$

$$\sigma^2 = gD_*(l^2 + k^2) + f_0^2. \tag{10.23e}$$

These are often called Sverdrup waves (apparently after Sverdrup, 1926). Rotation has made them dispersive and they propagate only when $\sigma^2 > f_0^2$. The group velocity $c_g = (\partial\sigma/\partial l, \partial\sigma/\partial k)$ is parallel to the wavenumber and rises from zero at $\sigma = f_0$ toward $(gD_*)^{1/2}$ as $\sigma^2 \gg f_0^2$. Dynamically these waves are LSW waves perturbed by rotation. Particle paths are ellipses with ratio f/σ of minor to major axis and with major axis oriented along (l, k). Particles traverse these paths in the clockwise direction (viewed from above) when $f > 0$ (northern hemisphere). Sverdrup waves are reflected specularly at a straight coast but with a phase shift; the sum

$$\zeta = a \exp(i\sigma t + ilx + iky)$$
$$+ a[(l\sigma + ikf_0)/(l\sigma - ikf_0)]$$
$$\times \exp(-i\sigma t - ilx + iky) \tag{10.24}$$

of two Sverdrup waves satisfies $u = 0$ at the coast $x = 0$, the angle $\tan^{-1}(k/l)$ of incidence equals the angle of reflection, and the reflected amplitude differs from the incident amplitude by the multiplicative constant $(l\sigma + ikf_0)/(l\sigma - ikf_0)$, which is complex but of modulus unity. The sum (10.24) is often called a *Poincaré wave*. The normal modes of a closed basin with perimeter P are the eigensolutions $Z_n(x,y)\exp(-i\sigma_n t)$, σ_n of

$$\nabla_2^2 Z_n + [(\sigma_n^2 - f_0^2)/gD_*]Z_n = 0 \tag{10.25}$$

with

$$-i\sigma_n \partial Z_n/\partial(\text{normal})$$
$$+ f_0 \partial Z_n/\partial(\text{tangent}) = 0 \quad \text{at} \quad P. \tag{10.26}$$

On account of the boundary condition (10.26), they are not usually separable functions of the two horizontal space coordinates. The circular basin (Lamb, 1932, §209-210) is an exception. Rao (1966) discusses the rectangular basin, but the results are not easily summarized. A salient feature, the existence of free oscillations with $\sigma^2 < f_0^2$, is rationalized below.

With rotation, Lord Kelvin (Thomson, 1879; Lamb, 1932, §208) showed that a coast not only reflects Sverdrup waves for which $\sigma^2 > f_0^2$, but makes possible a new kind of coastally trapped motion for which $\sigma^2 \gtrless f_0^2$. This Kelvin wave has the form

$$\zeta = a \exp[-i\sigma t + iky + k(f_0/\sigma)x], \tag{10.27a}$$

$$u = 0, \tag{10.27b}$$

$$v = (gk/\sigma)\zeta, \tag{10.27c}$$

$$w = -i\sigma(z/D_* + 1)\zeta, \tag{10.27d}$$

$$\sigma^2 = gD_*k^2 \tag{10.27e}$$

along the straight coast $x = 0$. The velocity normal to the coast vanishes everywhere in the fluid and not only

Myrl C. Hendershott

at the coast. The wave is dispersionless and propagates parallel to the shore with speed $(gD_*)^{1/2}$ for $\sigma^2 \gtrless f_0^2$ just like a longitudinal gravity wave but with an offshore profile $\exp[k(f_0/\sigma)x]$ that decays or grows exponentially seaward depending upon whether the wave propagates with the coast to its right or to its left (in the northern hemisphere, $f_0 > 0$). For vanishing rotation, the offshore decay or growth scale becomes infinite and the Kelvin wave reduces to an ordinary gravity wave propagating parallel to the coast. The Kelvin wave is dynamically exactly a LSW gravity wave in the longshore direction and is exactly geostrophic in the cross-shore direction.

A pair of Kelvin waves propagating in opposite directions along the two coasts of an infinite canal (at, say, $x = 0$ and $x = W$) gives rise to a pattern of sea-level variation in which the nodal lines that would occur without rotation shrink to amphidromic points, at which the surface neither rises nor falls and about which crests and troughs rotate counterclockwise (in the northern hemisphere) as time progresses. For equal-amplitude oppositely propagating Kelvin waves, the amphidromic points fall on the central axis of the canal and are separated by a half-wavelength (πk^{-1}). When the amplitudes are unequal, the line of amphidromes moves away from the coast along which the highest-amplitude Kelvin wave propagates. For a sufficiently great difference in amplitudes, the amphidromes may occur beyond one of the coasts, i.e., outside of the canal.

Such a pair of Kelvin waves cannot by themselves satisfy the condition of zero normal fluid velocity in a closed canal (say at $y = 0$). Taylor (1921) showed how this condition could be satisfied by adjoining to the pair of Kelvin waves an infinite sum of channel Poincaré modes

$$\zeta = [\cos(m\pi x/W) - (f_0/\sigma)(kW/m\pi)$$
$$\times \sin(m\pi x/W)] \exp[-i\sigma t \pm iky], \qquad (10.28)$$
$$\sigma^2 = (m^2\pi^2/W^2 + k^2)gD_* + f_0^2, \qquad m = 1, 2, \ldots,$$

each of which separately has vanishing normal fluid velocity at the channel walls $(x = 0, W)$. These are just the waveguide modes of the canal. Mode m decays exponentially away from the closure (is evanescent) if

$$\sigma^2 < f_0^2 + (m^2\pi^2/W^2)gD_*. \qquad (10.29)$$

If σ is so low, W so small, or D so great that all modes $m = 1, 2, \ldots$ are evanescent, then the Kelvin wave incident on the closure has to be perfectly reflected with at most a shift of phase. When (10.29) is violated for the one or more lowest modes, then some of the energy of the incident Kelvin wave is scattered into traveling Poincaré modes.

If (10.29) is satisfied for all m and if the decay scale $(gD_*)^{1/2}/f_0$ of the Kelvin waves is a good deal smaller

than the channel width W, then the Poincaré modes sum to an appreciable contribution only near the corners of the closure. The Kelvin wave then proceeds up the channel effectively hugging one coast, turns the corners of the closure with a phase shift [evaluated by Buchwald (1968) for a single corner], and returns back along the channel hugging the opposite coast. Now it becomes apparent that, with allowance for corner phase shifts, closed rotating basins have a class of free oscillation whose natural frequencies are effectively determined by fitting an integral number of Kelvin waves along the basin perimeter. Such free oscillations may have $\sigma^2 \lesssim f_0^2$. They are readily identified in Lamb's (1932, §209–210) normal modes of a uniform-depth circular basin.

10.4.3 The Effect of Density Stratification on Long Waves

All of the foregoing solutions are barotropic surface waves. Stokes (1847; Lamb, 1932, §231) pointed out that surface waves are dynamically very much like waves at the interfaces between fluid layers of differing densities. Allowance for continuous vertical variation of density was made by Rayleigh (1883). Lord Kelvin's plane model (10.18) must be extended to read

$$\frac{\partial u}{\partial t} - f_0 v = -\frac{1}{\bar{\rho}_0}\frac{\partial p}{\partial x}, \qquad (10.30a)$$

$$\frac{\partial v}{\partial t} + f_0 u = -\frac{1}{\bar{\rho}_0}\frac{\partial p}{\partial y}, \qquad (10.30b)$$

$$N^2 w = -\frac{1}{\bar{\rho}_0}\frac{\partial^2 p}{\partial z\, \partial t}, \qquad (10.30c)$$

$$\frac{\partial u}{\partial x} + \frac{\partial v}{\partial y} + \frac{\partial w}{\partial z} = 0, \qquad (10.30d)$$

with

$$w = 0 \qquad \text{at} \quad z = -D_* \qquad (10.31)$$

and

$$p = \bar{\rho}_0 g \zeta \qquad \text{at} \quad z = 0. \qquad (10.32)$$

Notation is as in (10.6).

For the case of constant depth D_*, the principal result is that the dependent variables have the separable form

$$(u,v,w,p) = \{U(x,y,t), V(x,y,t), W(x,y,t), Z(x,y,t)\}$$
$$\times \{F_u(z), F_u(z), F_w(z), F_p(z)\}^T \qquad (10.33)$$

where

$$W = \partial Z/\partial t,$$
$$F_u = F_p/\bar{\rho}_0 g = D_n\, \partial F_w/\partial z, \qquad (10.34)$$

and

$$\frac{\partial U}{\partial t} - f_0 V = -g \frac{\partial Z}{\partial x}, \tag{10.35a}$$

$$\frac{\partial V}{\partial t} + f_0 U = -g \frac{\partial Z}{\partial y}, \tag{10.35b}$$

$$\frac{\partial Z}{\partial t} + D_n \left(\frac{\partial U}{\partial x} + \frac{\partial V}{\partial y} \right) = 0, \tag{10.35c}$$

with

$$\frac{\partial^2 F_w}{\partial z^2} + \frac{N^2(z)}{gD_n} F_w = 0, \tag{10.36}$$

$$F_w = 0 \quad \text{at} \quad z = -D_*, \tag{10.37}$$

$$F_w - D_n \partial F_w/\partial z = 0 \quad \text{at} \quad z = 0. \tag{10.38}$$

According to (10.35), the horizontal variations of all quantities are exactly as in the homogeneous flat bottom case except that now the apparent depth D_n is obtained by solving the eigenvalue problem (10.36) for the vertical structure. Typically (10.36) yields a barotropic mode $F_{w0} \simeq z + D_*$, $D_0 \simeq D_*$ plus an infinite sequence of baroclinic modes F_{wn} characterized by n zero crossings (excluding the one at $z = -D_*$) and by very small equivalent depths D_n. Baroclinic WKB approximate solutions (10.36)–(10.38) are

$$F_{wn}(z) = N^{-1/2}(z) \sin\left[(1/gD_n)^{1/2} \int_{-D_*}^{z} N(z') dz' \right],$$
$$D_n = \left[\int_{-D_*}^{0} N(z') dz' \right]^2 \Big/ (gn^2\pi^2). \tag{10.39}$$

These are exact for constant buoyancy frequency N_0. For $D_* = 4000$ m and $N_0 = 10\Omega$, $D_n = (0.1/n^2)$ m. When $N(z) = N_0$, it is easy to show that

[w at the free surface/interior maximum value

of w] $= N_0^2 D_*/n\pi g \ll 1$. \tag{10.40}

Free surface variation is thus qualitatively and quantitatively unimportant for baroclinic modes. They are therefore usually called internal modes.

In a flat-bottomed ocean, stratification is thus seen to make possible an infinite sequence of internal replicas of the barotropic LSW gravity waves, Sverdrup waves, Poincaré waves, Kelvin waves, and basin normal modes discussed above. All these except the Kelvin waves have $\sigma^2 > f_0^2$. They must also have $\sigma^2 < N^2(z)$ over part of the water column, although the present treatment does not make this obvious because $\sigma^2 \ll N^2$ is always assumed. The horizontal variation of these replicas is governed by the equations describing the barotropic mode, except that the depth D_n is a small fraction of the actual (constant) depth D_*. Without rotation, the speed of barotropic long gravity waves is $(gD_*)^{1/2} \simeq 200$ m s^{-1} in the deep sea. Long internal gravity waves move at the much slower $(gD_n)^{1/2} \simeq$

$(1/n)$ m s^{-1}. For comparable frequencies, the internal waves thus have much shorter wavelength than the surface wave.

An important point is that the separation of variables (10.33) works in spherical coordinates as well as in Cartesian coordinates, provided only that the depth is constant. The horizontal variation of flow variables is then governed by LTE with appropriate equivalent depth D_n given by (10.36)–(10.38).

For plane waves of frequency σ, relaxation of $N^2 \gg \sigma^2$ leads to the replacement of (10.36) by

$$\frac{\partial^2 F_w}{\partial z^2} + \frac{[N^2(z) - \sigma^2]}{gD_n} F_w = 0. \tag{10.41}$$

High-frequency waves, for which $[N^2(z) - \sigma^2]$ changes sign over the water column, are discussed in chapter 9.

The simplicity of these flat-bottom results is deceptive, because they are very difficult to generalize to include bottom relief. The reason for this is most easily seen by eliminating (u, v) from (10.30) for harmonic motion $[\exp(-i\sigma t)]$ to obtain a single equation in w:

$$\frac{\partial^2 w}{\partial z^2} - \left(\frac{N_0^2}{\sigma^2 - f_0^2} \right) \left(\frac{\partial^2 w}{\partial x^2} + \frac{\partial^2 w}{\partial y^2} \right) = 0. \tag{10.42}$$

This equation is hyperbolic in space for internal waves (for which $f_0^2 < \sigma^2 < N_0^2$). Its characteristic surfaces are

$$z = \pm(x^2 + y^2)^{1/2}(\sigma^2 - f_0^2)^{1/2}/N_0. \tag{10.43}$$

Solutions of (10.42) may be discontinuous across characteristic surfaces, and they depend very strongly upon the relative slope of characteristics and bounding surfaces. Without rotation, internal waves of frequency σ are solutions of the hyperbolic equation

$$\frac{\partial^2 p}{\partial z^2} - \frac{(N_0^2 - \sigma^2)}{\sigma^2} \left(\frac{\partial^2 p}{\partial x^2} + \frac{\partial^2 p}{\partial y^2} \right) = 0 \tag{10.44}$$

with the simple condition

$$\frac{\partial p}{\partial n} = 0 \quad \text{at solid boundaries.} \tag{10.45}$$

For closed boundaries (i.e., a container filled with stratified fluid) this is an ill-posed problem in the sense that tiny perturbations of the boundaries may greatly alter the structure of the solutions. Horizontal boundaries, although analytically tractable, are a very special case.

10.4.4 Rossby and Planetary Waves

In an influential study whose emphasis upon physical processes marks the beginning of the modern period, Rossby and collaborators (1939) rediscovered Hough's second-class oscillations and suggested that they might be of great importance in atmospheric dynamics (see also chapters 11 and 18).

Myrl C. Hendershott

Perhaps of even greater influence than this discovery was Rossby's creation of a new plane model. It amounts to LTE written in the Cartesian coordinates

$$x = (a \cos \theta_0)(\phi - \phi_0), \qquad y = a(\theta - \theta_0) \qquad (10.46)$$

tangent to the sphere at (ϕ_0, θ_0). Rossby's creative simplification was to ignore the variation of all metric coefficients $(\cos \theta = \cos \theta_0)$ and to retain the latitude variation of

$$f = 2\Omega \sin \theta \simeq 2\Omega \sin \theta_0 + y(2\Omega/a) \cos \theta_0$$
$$= f_0 + \beta y \qquad (10.47)$$

only when f is explicitly differentiated with respect to y. Rossby's notation

$$\beta \equiv \partial f/\partial y \qquad (10.48)$$

has since become almost universal. Such Boussinesq-like approximations to the spherical equations are usually called β-plane equations.

Rossby's original approximation, which I shall call Rossby's β-plane, further suppressed horizontal divergence $(\zeta = 0)$. It yields rational approximations (Miles, 1974b) for second-class solutions of LTE whose horizontal scale is much smaller than the earth's radius. A quite different approximation yielding rational approximations for both first- and second-class solutions of LTE when they are equatorially trapped is the equatorial β-plane (see section 10.4.5). Both Rossby's β-plane equations and the equatorial β-plane equations differ from those obtained by the often encountered procedure of making Rossby's simplification but retaining divergence. This results in what I shall call simply the β-plane equations, in conformity with common usage. It is a rational approximation to LTE only at low $(\sigma^2 \ll f_0^2)$ frequencies and is otherwise best regarded as a model of LTE.

Without divergence, the homogeneous LTE (10.30) may be cross-differentiated to yield a vorticity equation

$$\frac{\partial \nabla_{2s}^2 \psi}{\partial t} + 2\Omega \frac{\partial \psi}{\partial \phi} = 0$$
$$\left[\nabla_{2s}^2 \equiv \frac{1}{a^2 \cos^2 \theta} \frac{\partial^2}{\partial \phi^2} + \frac{1}{a^2 \cos \theta} \frac{\partial}{\partial \theta} \left(\cos \frac{\partial}{\partial \theta} \right) \right] \qquad (10.49)$$

here written in terms of a streamfunction ψ defined by

$$v \cos \theta = \partial \psi/\partial \phi, \qquad u = -\partial \psi/\partial \theta. \qquad (10.50)$$

Rossby's β-plane approximation to this, obtained by locally approximating the spherical Laplacian ∇_{2s}^2 as the plane Laplacian and going to the locally tangent coordinates (10.46), is

$$\frac{\partial \nabla_2^2 \psi}{\partial t} + \beta \frac{\partial \psi}{\partial x} = 0, \qquad (10.51)$$

where

$$v = \partial \psi/\partial x, \qquad u = -\partial \psi/\partial y. \qquad (10.52)$$

The spherical vorticity equation (10.49) has as everywhere bounded solutions

$$\psi = S_n(\phi', \theta'), \qquad S_n(\phi, \theta) \equiv P_n^l(\sin \theta) \exp(il\phi), \qquad (10.53)$$

where (ϕ', θ') are spherical coordinates relative to a pole P' displaced an arbitrary angle from the earth's pole P of rotation and rotating about P with angular velocity

$$c = -2\Omega/[n(n + 1)] \qquad (10.54)$$

(Longuet-Higgins, 1964). When $P' = P$, (10.54) is exactly the second part of (10.17); these *are* Hough's second-class oscillations. Rossby's β-plane equivalents are

$$\psi = Z_n(x - ct, y), \qquad \nabla_2^2 Z_n + \lambda_n^2 Z_n = 0, \qquad (10.55)$$

where $c = -\beta/\lambda_n^2$.

Plane Rossby waves are the particular case

$$\psi = a \exp(-i\sigma t + ilx + iky), \qquad (10.56)$$
$$\sigma = -\beta l/(l^2 + k^2). \qquad (10.57)$$

They are transverse $[(u, v)$ perpendicular to $(l, k)]$ and dispersive, with the propagation of phases always having a westward component $(\sigma/l < 0)$. Their frequencies are typically low relative to f_0. Since σ depends both on wavelength and wave direction, these waves do not reflect specularly at a straight coast. Longuet-Higgins (1964) gives an elegant geometrical interpretation (figure 10.1) of their dispersion relation (10.57) and shows that it is the group velocity $(\partial \sigma/\partial l, \partial \sigma/\partial k)$ that reflects specularly in this case (figure 10.2).

Rossby-wave normal modes of a closed basin of perimeter P have the form (Longuet-Higgins, 1964)

$$\psi = Z_n(x, y) \exp[-i\sigma_n t - i(\beta/2\sigma_n)x], \qquad (10.58)$$
$$\sigma_n = \beta/2\lambda_n \qquad (10.59)$$

where

$$\nabla_2^2 Z_n + \lambda_n^2 Z_n = 0, \qquad Z_n = 0 \quad \text{on} \quad P. \qquad (10.60)$$

These Rossby-wave normal modes are in remarkable contrast with the gravity-wave normal modes of the same basin without rotation:

$$\zeta_n = Z_n(x, y) \exp(-i\sigma_n t), \qquad (10.61)$$
$$\sigma_n = \lambda_n (gD_*)^{1/2} \qquad [\partial Z_n/\partial(\text{normal}) = 0 \text{ on } P]. \qquad (10.62)$$

The gravity-wave modes have a lowest-frequency $(n = 1)$ grave mode and the spatial scales of higher-frequency modes are smaller. The Rossby-wave modes have a highest frequency $(n = 1)$ mode and the spatial scales of lower frequency modes are smaller.

The physical mechanism that makes Rossby waves possible is most easily seen for nearly zonal waves $(\partial/\partial y \ll \partial/\partial x)$. Then Rossby's vorticity equation (10.51) becomes

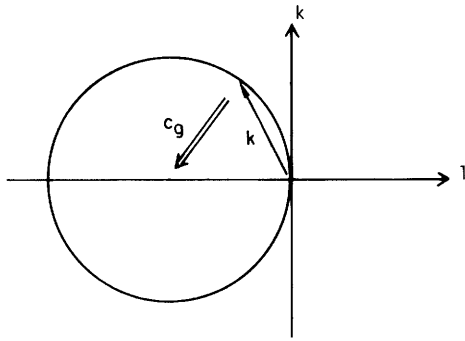Figure 10.1 The locus of wavenumbers $k = (k,l)$ allowed by the Rossby dispersion relation (10.57)

$$(l + \beta/2\sigma)^2 + k^2 = (\beta/2\sigma)^2$$

is a circle of radius $\beta/2\sigma$ centered at $(-\beta/2\sigma, 0)$. The group velocity vector $\mathbf{c_g} = (\partial\sigma/\partial l, \partial\sigma/\partial k)$ points from the tip of the wavenumber vector toward the center of the circle and has magnitude $|\mathbf{c_g}| = \beta/(l^2 + k^2)$.
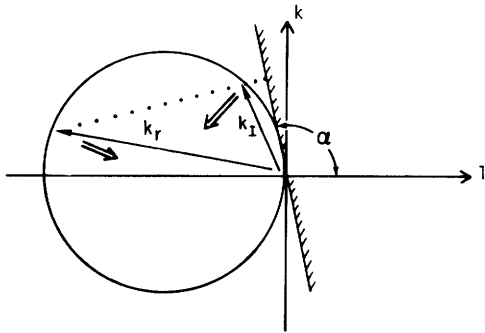

Figure 10.2 A Rossby wave with wavenumber $\mathbf{k_i}$ is incident on a straight coast inclined at an angle α to the east-west direction. The wavenumber $\mathbf{k_r}$ of the reflected wave is fixed by the necessity that $\mathbf{k_i}$ and $\mathbf{k_r}$ have equal projection along the coast. The group velocity reflects specularly in the coast.
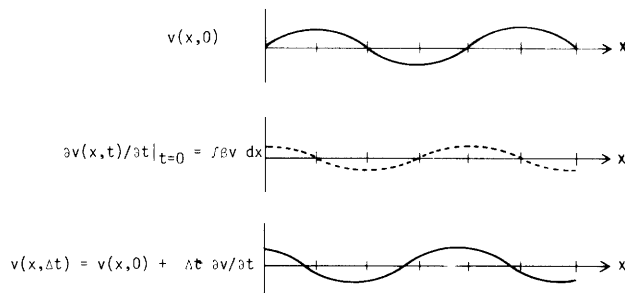
Figure 10.3 The flow $v(x, t)$ evolving from the initial flow $v(x, 0) \sim \sin(lx)$ as fluid columns migrate north-south (and so exchange planetary and relative vorticity) is a westward displacement of the initial flow. Notice that although parcels take on clockwise-counterclockwise relative vorticity as they are moved north-south, the westward displacement is not the result of advection of vorticity of one sign by the flow associated with the other as is the case in a vortex street.

$$\frac{\partial^2 v}{\partial x\, \partial t} + \beta v = 0. \tag{10.63}$$

North-south motions v result in changes in the local vorticity $\partial v/\partial x$. When the initial north-south motion is periodic in x, then examination (figure 10.3) of (10.63) shows that the additional north-south motion generated by the vorticity resulting from the initial pattern of north-south motion combines with that pattern to shift it westward, in accordance with (10.57).

Rossby's vorticity equation (10.51) corresponds to the plane equations

$$\frac{\partial u}{\partial t} - fv = -\frac{1}{\rho_0}\frac{\partial p}{\partial x}, \tag{10.64a}$$

$$\frac{\partial v}{\partial t} + fu = -\frac{1}{\rho_0}\frac{\partial p}{\partial y}, \tag{10.64b}$$

$$\frac{\partial u}{\partial x} + \frac{\partial v}{\partial y} = 0, \tag{10.64c}$$

$$f = f_0, \qquad \partial f/\partial y = \beta, \tag{10.64d}$$

so that Rossby's solutions are almost geostrophic $(\sigma \ll f_0)$ and perfectly nondivergent. The absence of divergence and vertical velocity is an extreme of the tendency, in quasigeostrophic flow, for the vertical velocity to be order Rossby number $(\ll 1)$ smaller than a scale analysis of the continuity equation would indicate (Burger, 1958). This tendency is absent at planetary length scales, and Rossby's β-plane (10.64) correspondingly requires modification.

Remarkably, Rossby and collaborators (1939) prefaced their analysis with a resumé of a different physical mechanism due to J. Bjerknes (1937), a mechanism that also results in westward-propagating waves but for a different reason, and that supplies the modification of Rossby's β-plane required at planetary scales. The plane equations corresponding to Rossby's summary of Bjerknes' arguments are

$$-fv = -g\frac{\partial\zeta}{\partial x}, \tag{10.65a}$$

$$fu = -g\frac{\partial\zeta}{\partial y}, \tag{10.65b}$$

$$\frac{\partial\zeta}{\partial t} + D_*\left(\frac{\partial u}{\partial x} + \frac{\partial v}{\partial y}\right) = 0, \tag{10.65c}$$

$$f = f_0, \qquad \partial f/\partial y = \beta. \tag{10.65d}$$

By physical arguments (figure 10.4), Bjerknes deduced that an initial pressure perturbation would always propagate westward. The corresponding analysis of (10.65) is to form an elevation equation

$$\frac{\partial\zeta}{\partial t} - (gD_*\beta/f_0^2)\frac{\partial\zeta}{\partial x} = 0 \tag{10.66}$$

and to note that it has the dispersionless solutions

302
Myrl C. Hendershott

$\zeta = F[x + (gD_*\beta/f_0^2)t, y]$,

where $F(x, y)$ is the initial pressure perturbation. In particular,

$$\zeta = a \exp(-i\sigma t + ilx + iky), \tag{10.67}$$

$$\sigma = -(gD_*\beta/f_0^2)l. \tag{10.68}$$

All solutions travel westward at $(gD_*\beta/f_0^2)^{1/2}$. These motions, according to (10.65), are perfectly geostrophic but divergent.

More complete analysis (Longuet-Higgins, 1964) shows that the two dispersion relations (10.57) of Rossby and (10.68) of Bjerknes are limiting cases of the β-plane dispersion relation

$$\sigma = -\beta l/(l^2 + k^2 + f_0^2/gD_*) \tag{10.69}$$

for second-class waves displayed in figure 10.5. It would be appropriate to call the two kinds of second-class waves Rossby and Bjerknes waves, respectively, but in practice both are commonly called Rossby waves. I shall distinguish them as short, nondivergent and long, divergent Rossby waves.

When divergence is allowed, the (constant) depth D_* enters the dispersion relation (10.69) in the length scale

$$a_R = (gD_*/f_0^2)^{1/2}, \tag{10.70}$$

usually called the Rossby radius. There is not one Rossby radius, but rather there are many, since the constant-depth barotropic second-class waves so far discussed have an infinite sequence of baroclinic counterparts with $D_* = D_n$, $n = 1, \ldots$, given by (10.36)-(10.39). Waves longer than the Rossby radius are long, divergent Rossby waves; those shorter than the Rossby radius are short, nondivergent Rossby waves.

The barotropic Rossby radius $a_{Ro} = (gD_0/f_0^2)^{1/2}$ has $D_0 \simeq D_*$ and is thus the order of the earth's radius. Barotropic Rossby waves are consequently relatively high-frequency (typically a few cycles per month) waves and they are able to traverse major ocean basins in days to weeks. Baroclinic Rossby radii $a_{Rn} = (gD_n/f_0^2)^{1/2}$ are the order of 10^2 km or less in mid-latitudes. Baroclinic mid-latitude Rossby waves are consequently relatively low-frequency waves and would take years to traverse major mid-latitude basins. In the tropics, f_0 becomes small and baroclinic Rossby waves speed up to the point where they could traverse major basins in less than a season. But a different discussion is really necessary for the tropics (see chapter 6).

Rossby advanced his arguments to rationalize the motion of mid-latitude atmospheric pressure patterns. In both atmosphere and ocean, the slowness and relatively small scale of most second-class waves must make their occurrence in "pure" form very rare. Oceanic measurements from the MODE experiment
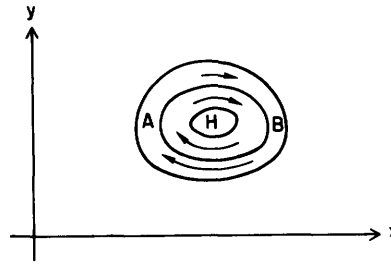

Figure 10.4 If the flow is totally geostrophic but the Coriolis parameter increases with latitude, then the flow at A converges because the geostrophic transport between a pair of isobars south of H is greater than that between the same pair north of H. By (10.65c), pressure thus rises at A. Similarly, the flow at B diverges and pressure there drops. The initial pattern of isobars is then shifted westward.
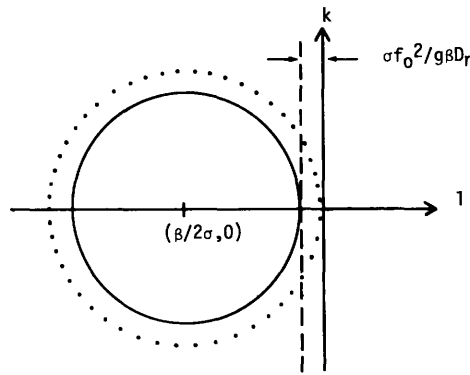

Figure 10.5 The locus of wavenumbers (l, k) allowed by the β-plane dispersion relation (10.69) for second-class waves

$$(l + \beta/2\sigma)^2 + k^2 = (\beta/2\sigma)^2 - (f_0^2/gD_n)$$

is a circle(———) whose radius is $[(\beta/2\sigma)^2 - (f_0^2/gD_n)]^{1/2}$ centered at $(-\beta/2\sigma, 0)$. Dotted circle $(\cdots)$ is the Rossby dispersion relation (10.57) for short waves. Dashed line (---) is the Bjerknes dispersion relation (10.68) appropriate for long waves. The scale a_R dividing short and long waves is

$$a_R = [2(\beta/2\sigma)(\sigma f_0^2/\beta gD_n)]^{-1/2}.$$

do show, however, characteristics of both short baroclinic (figure 10.6) and long barotropic (figure 10.7) Rossby waves.

The oscillations having the two dispersion relations (10.23e) with $D_* = D_n$ for first-class waves and (10.69) for second-class waves are mid-latitude plane-wave approximations of solutions of LTE. Figure 10.8 plots the two dispersion relations together. A noteworthy feature is the frequency interval between f_0 and $(\beta/2f_0)(gD_n)^{1/2}$ within which no plane waves propagate. Taken at face value, this gap suggests that velocity spectra should show a valley between these two frequencies with a steep high-frequency $[f_0]$ wall and a rather more gentle low-frequency $[(\beta/2f_0)(gD_n)^{1/2}, n = 0,1,2, \ldots]$ wall. Such a gap is indeed commonly observed; but the dynamics of the low frequencies are almost surely more complex than those of the linear β-plane. The latitude dependence implicit in the definition of f_0 and β is consistent with equatorial trapping of low-frequency first-class waves and high-frequency second-class waves. This is more easily seen in approximations, such as the following, which better acknowledge the earth's sphericity.

10.4.5 The Equatorial β-Plane

For constant depth D_*, the homogeneous LTE (10.5) may be equatorially approximated by expanding all variable coefficients in θ and then neglecting $\theta^2, \theta^3, \ldots$. The resulting equatorial β-plane equations are

$$\frac{\partial u}{\partial t} - \beta y v = -g\frac{\partial \zeta}{\partial x}, \tag{10.71a}$$

$$\frac{\partial v}{\partial t} + \beta y u = -g\frac{\partial \zeta}{\partial y}, \tag{10.71b}$$

$$\frac{\partial \zeta}{\partial t} + D_*\left(\frac{\partial u}{\partial x} + \frac{\partial v}{\partial y}\right) = 0, \tag{10.71c}$$

where $x = a\phi$, $y = a\theta$, and $\beta = 2\Omega/a$. They govern both barotropic and baroclinic motions provided that D_* is interpreted as the appropriate equivalent depth D_n defined by (10.36)-(10.38). Moore and Philander (1977) and Philander (1978) give modern reviews.

Solutions of these equations can be good approximations to solutions of LTE only when they decay very rapidly away from the equator. But the qualitative nature of their solutions, bounded as $y \to \pm\infty$, closely resembles solutions of LTE bounded at the poles, even
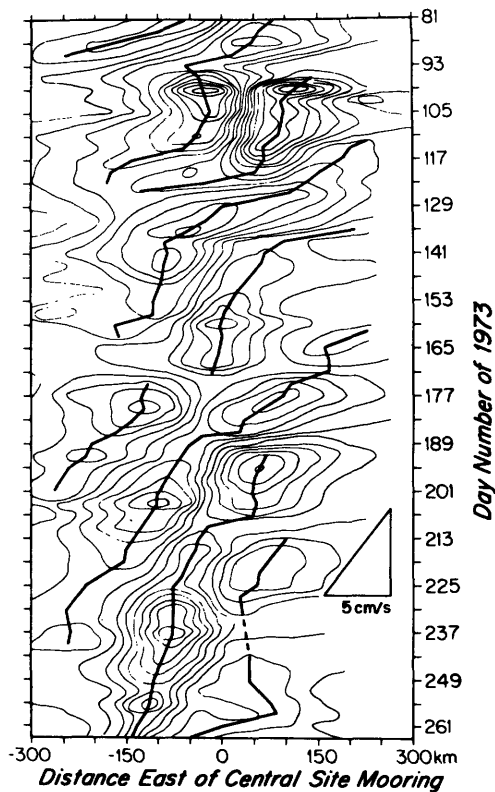

Figure 10.6A Time–longitude plot of streamfunction inferred from objective maps of 1500-m currents along 28°N (centered at 69°49'W) by Freeland, Rhines and Rossby (1975). There is evidence of westward propagation of phases. Currents at this depth are not dominated by "thermocline eddies" (section 10.4.7) but are representative of the deep ocean.
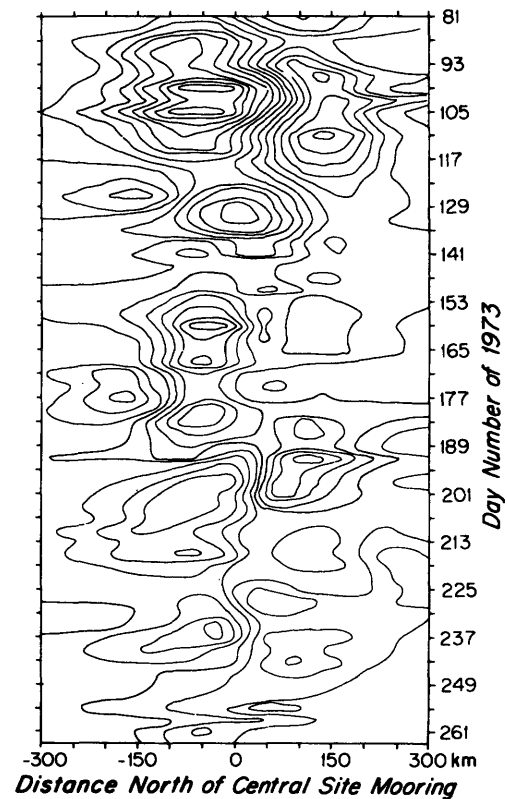
Figure 10.6B As figure 10.6A but in time–latitude plot along 69°40'W. There is no evidence for a preferred direction of latitudinal phase propagation. (Rhines, 1977.)
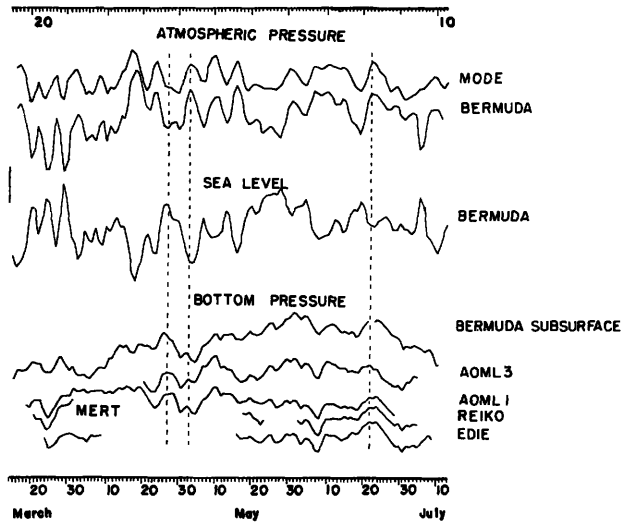
Myrl C. Hendershott

Figure 10.7 Time series of bottom pressure in MODE (Brown et al., 1975). The cluster of named gauges centered at 28°N, 69°40'W show remarkable coherence despite 0 (180-km) separation, and all are coherent with the (atmospheric pressure corrected) sea level at Bermuda (650 km distant, labeled Bermuda bottom). (Brown et al., 1975.)
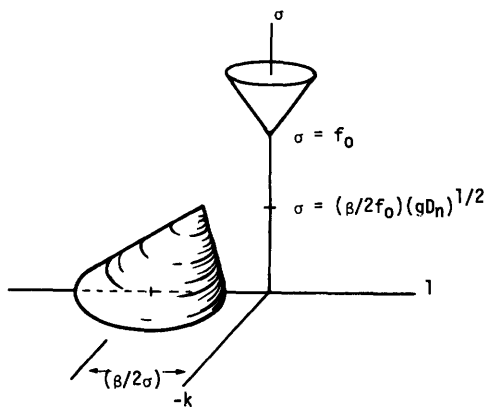

Figure 10.8 The f-plane dispersion relation

$$\sigma^2 = f_0^2 + gD_n(l^2 + k^2)$$

for first-class waves allows no waves with $\sigma^2 < f_0^2$. The β-plane dispersion relation

$$\sigma = -\beta l/[l^2 + k^2 + f_0^2/gD_n]$$

for second-class waves allows no waves with $\sigma > (\beta/2f_0)(gD_n)^{1/2}$.

when the equatorial approximation is transgressed. Historically these approximate solutions provided a great deal of insight into the latitudinal variation of solutions of LTE.

Most of the solutions are obtainable from the single equation that results when u, ζ are eliminated from (10.71). With

$$v = V(y) \exp(-i\sigma t + ilx) \tag{10.72}$$

that equation is

$$\frac{\partial^2 V}{\partial y^2} + \left[\left(\frac{\sigma^2}{gD_*} - l^2 - \frac{l\beta}{\sigma} \right) - \frac{\beta^2}{gD_*} y^2 \right] V = 0. \tag{10.73}$$

It also occurs in the quantum-mechanical treatment of the harmonic oscillator. Solutions are bounded as $y \rightarrow \pm\infty$ only if

$$\left(\frac{\sigma^2}{gD_*} - l^2 - \frac{l\beta}{\sigma} \right) = (2m + 1) \frac{\beta}{(gD_*)^{1/2}},$$

$$m = 0, 1, 2, \ldots, \tag{10.74}$$

and they are then

$$V(y) = H_m[y\beta^{1/2}/(gD_*)^{1/4}] \exp[-y^2\beta/2(gD)^{1/2}], \tag{10.75}$$

wherein the H_m are Hermite polynomials $(H_0(z) = 1, H_1(z) = z, \ldots)$.

The remaining solution may be taken to be $v = 0$ with $m = -1$ in (10.74). It is obtained by solving (10.71) with $v = 0$. The solution bounded as $y \rightarrow \pm\infty$ is

$$\zeta = \exp[-i\sigma t + ilx - (\beta l/\sigma)y^2/2] \tag{10.76}$$

with

$$l = \sigma/(gD_*)^{1/2} \tag{10.77}$$

[(10.77) is (10.74) with $m = -1$].

The very important dispersion relation (10.74) with $m = -1, 0, 1, \ldots$ thus governs all the equatorially trapped solutions of (10.71). Introducing the dimensionless variables $\omega, \lambda, \zeta, \eta$ defined by

$$\sigma = \omega(2\Omega\Lambda^{-1/4}), \qquad l = \lambda(a^{-1}\Lambda^{1/4}), \tag{10.78}$$

$$(x, y) = (\xi, \eta)(a\Lambda^{-1/4}), \qquad t = \tau[(2\Omega)^{-1}\Lambda^{1/4}]$$

$(\Lambda = 4\Omega^2 a^2/gD_*)$ allows us to rewrite (10.73) and its solutions (10.72), (10.75), (10.76) as

$$\frac{\partial^2 V}{\partial \eta^2} + [(\omega^2 - \lambda^2 - \lambda/\omega) - \eta^2]V = 0, \tag{10.79}$$

$$v = H_m(\eta) \exp(-i\omega\tau + i\lambda\xi - \eta^2/2),$$

$$m = 0, 1, \ldots, \tag{10.80}$$

$$\zeta = \exp[-i\omega\tau + i\lambda\xi - (\lambda/\omega)\eta^2/2], \qquad m = -1, \tag{10.81}$$

while the dispersion relation (10.74) becomes

$$\omega^2 - \lambda^2 - \lambda/\omega = 2m + 1, \qquad m = -1, 0, 1, \ldots \quad (10.82)$$

These forms allow easy visualization of the solutions and permit a concise graphical presentation of the dispersion relation (figure 10.9).

The dispersion relation is cubic in σ (or ω) for given values of l (or λ) and m. For $m > 1$ the three roots correspond precisely to two oppositely traveling waves of the first class plus a single westward-traveling wave of the second class. The case $m = 0$ (Yanai, or Rossby-gravity, wave) is of first class when traveling eastward but of second class when traveling westward. The case $m = -1$ is an equatorially trapped Kelvin wave, dynamically identical to the coastally trapped Kelvin wave (10.27) in a uniformly rotating ocean.

The most useful aspect of these exact solutions is their provision of a readily understandable dispersion relation [(10.74) or (10.82)]. The latitudinal variation of flow variables is more readily discussed in terms of WKB solutions of (10.73). One can easily see *the* salient feature of the solutions, a transition from oscillatory to exponentially decaying latitudinal variation as the turning latitudes y_T of (10.73) (at which the coefficient [ ] of that equation vanishes), are crossed poleward. For waves of the first class, the term $l\beta/\sigma$ is small relative to the other terms in the dispersion relation and in the coefficient [ ]. The corresponding turning latitudes $y_T^{(1)}$ are therefore approximately given by

$$[y_T^{(1)}]^2 = (\sigma/\beta)^2[1 - l^2(gD_*)/\sigma^2] < (\sigma/\beta)^2. \quad (10.83)$$
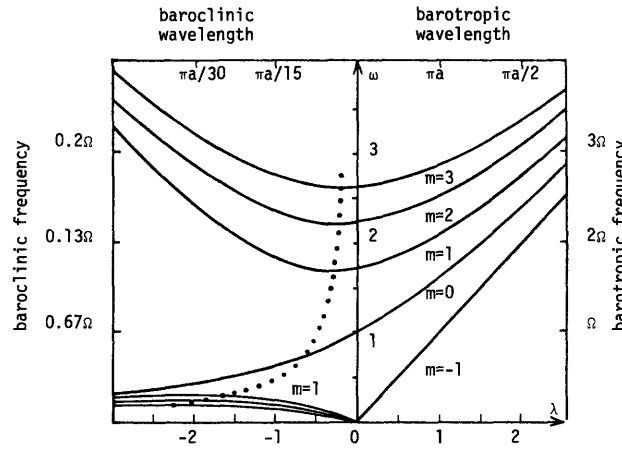

baroclinic wavelength   barotropic wavelength

Figure 10.9 The equatorial β-plane dispersion relation (10.82)

$$\omega^2 - \lambda^2 - \lambda/\omega = 2m + 1.$$

Dimensional wavelengths and frequencies are obtained from the scaling (10.78) and are given for the barotropic mode ($D_0 = 4000$ m, $\Lambda = 20$) and for the first baroclinic mode ($D_0 = 0.1$ m, $\Lambda = 10^6$). For all curves but $m = 0$, intersections with dotted curve are zeros of group velocity.

For waves of the second class, the term σ^2/gD_* is small relative to the other terms in the dispersion relation and in the coefficient [ ]. The corresponding turning latitudes $y_T^{(2)}$ are therefore approximately given by

$$[y_T^{(2)}]^2 = (gD_*/\beta^2)(-l^2 - l\beta/\sigma) < gD_*/4\sigma^2. \quad (10.84)$$

Increasingly low-frequency waves of the first class and increasingly high-frequency waves of the second class are thus trapped increasingly close to the equator.

Only first-class waves having frequency greater than the inertial frequency βy penetrate poleward of latitude y [by (10.83)]. Only second-class waves having frequency below the cutoff frequency $(gD_*/4y^2)^{1/2}$ penetrate poleward of latitude y [by (10.84)]. This frequency-dependent latitudinal trapping corresponds to the mid-latitude frequency gap between first- and second-class waves discussed in the previous section and illustrated in figure 10.8. The correspondence correctly suggests that trapping and associated behavior characterize slowly varying (in the WKB sense) packets of waves propagating over the sphere as well as the globally standing patterns corresponding to the Hermite solutions (10.75). Waves thus need *not* be globally coherent to exhibit trapping and the features associated with it.

Near the trapping latitudes, (10.73) becomes

$$\frac{\partial^2 V}{\partial y^2} + (-2\beta^2 y_T/gD_*)(y - y_T)V = 0. \quad (10.85)$$

The change of variable $\eta = (2\beta^2 y_T/gD_*)^{1/3}(y - y_T)$ reduces this to Airy's equation

$$\frac{\partial^2 V}{\partial \eta^2} - \eta V = 0, \quad (10.86)$$

whose solution $Ai(\eta)$ bounded as $\eta \to \infty$ is plotted in figure 10.10. This solution has two important features: (1) gentle amplification (like $\eta^{-1/4}$) of the solution as the turning latitude ($\eta = 0$) is approached from the equator; and (2) transition from oscillatory to exponentially decaying behavior in a region $\Delta\eta$ of order roughly unit width surrounding the turning latitude. Consequently the interval Δy over which the solution of (10.85) changes from oscillatory to exponential behavior is $\Delta y = [2\beta^2 y_T/gD_*]^{-1/3}\Delta\eta$ or, since $\beta = 2\Omega/a$ and $\Delta\eta \approx 1$,

$$\Delta y = a(\Lambda\sigma/2\Omega)^{-1/3} \quad (10.87)$$

$$= a(2^{-1/2}\Lambda^{-1/2}\sigma/2\Omega)^{1/3} \quad (10.88)$$

for maximally penetrating first- and second-class waves. For diurnal ($\sigma = \Omega$) first-class barotropic ($\Lambda = 20$) waves, $\Delta y \approx 0.5a$; for diurnal first-class baroclinic ($\Lambda \approx 10^6$) waves, $\Delta y \approx 0.013a$. For 10-day ($\sigma = 0.1\Omega$) second-class barotropic waves, $\Delta y \approx 0.25a$. For 1-month
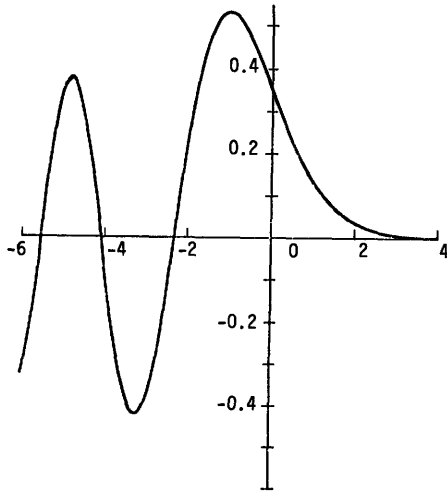
Myrl C. Hendershott

Figure 10.10 The Airy function Ai.

$(\sigma \simeq .03\Omega)$ second-class baroclinic waves, $\Delta y = 0.03a$. We thus obtain the important result that barotropic modes are not noticeably trapped (Δy is a fair fraction of the earth's radius and the Airy solution is only qualitatively correct anyway) but baroclinic modes are abruptly trapped (Δy is a few percentage points of the earth's radius).

The abrupt trapping of baroclinic waves at their inertial latitudes means that the Airy functions may describe quite accurately the latitude variation of near-inertial motions. Munk and Phillips (1968) and Munk (chapter 9) discuss the structure.

The clearest observations of equatorial trapping are by Wunsch and Gill (1976), from whose paper figure 10.11 is taken. Longer-period fluctuations at and near the equator have been observed, but their relation to the trapped solutions is not yet clear.

When an equatorially trapped westward-propagating wave meets a north–south western boundary (at, say, $x = 0$) it is reflected as a superposition of finite numbers of eastward-propagating waves including the Kelvin ($m = -1$) and Yanai ($m = 0$) waves (Moore and Philander, 1977). But when an equatorially trapped eastward-propagating wave meets a north–south eastern boundary, some of the incident energy is scattered into a poleward-propagating coastal Kelvin wave (10.29) and thus escapes the equatorial region (Moore, 1968). In latitudinally bounded basins, the requirement that solutions decay exponentially away from the equator is replaced by the vanishing of normal velocity at the boundaries. Modes closely confined to the equator will not be greatly altered by such boundaries; modes that have appreciable extraequatorial amplitude will behave like the β-plane solutions of sections 10.4.1–10.4.4 near the boundaries. A theory of free oscillations in idealized basins on the equatorial β-plane could be constructed on the basis of such observations, but powerful techniques for dealing with the spherical problem now exist (section 10.4.8).

10.4.6 Barotropic Waves over Bottom Relief

Stokes (1846; Lamb, 1932, §260) had shown that shoaling relief results in the trapping of an edge wave whose amplitude decays exponentially away from the coast, but the motion was not thought to be important.

Eckart (1951) solved the shallow-water equations [(10.18) with $f_0 = 0$] with the relief $D = ax$. Solutions of the form

$$\zeta = h(x)\exp(-i\sigma t + iky) \tag{10.89}$$

are governed by

$$x\frac{\partial^2 h}{\partial x^2} + \frac{\partial h}{\partial x} + [\sigma^2/(ag) - xk^2]h = 0. \tag{10.90}$$

Solutions of this are bounded as $x \to \infty$ only if

$$\sigma^2 = k(2n + 1)ag, \qquad n = 0, 1, \ldots, \tag{10.91}$$

and they are then

$$h(x) = L_n(2kx)\exp(-kx), \tag{10.92}$$

where the L_n are Laguerre polynomials [$L_0(z) = 1$, $L_1(z) = z - 1, \ldots$]. The $n = 0$ mode corresponds to Stokes's (1846) edge wave.

Eckart's solutions are LSW gravity waves refractively trapped near the coast by the offshore increase in shallow water wave speed $(gax)^{1/2}$. The Laguerre solutions (10.92) are correspondingly trigonometric shoreward of the turning points x_T at which the coefficient [ ] of (10.90) vanishes, and decay exponentially seaward.

Eckart's use of the LSW equations is not entirely self-consistent, since $D = ax$ increases without limit. Ursell (1952) removed the shallow-water approximation by completely solving

$$\frac{\partial^2 \phi}{\partial z^2} + \frac{\partial^2 \phi}{\partial x^2} - k^2\phi = 0 \tag{10.93}$$

subject to

$$\frac{\partial \phi}{\partial z} = (\sigma^2/g)\phi \qquad \text{at} \quad z = 0 \tag{10.94}$$
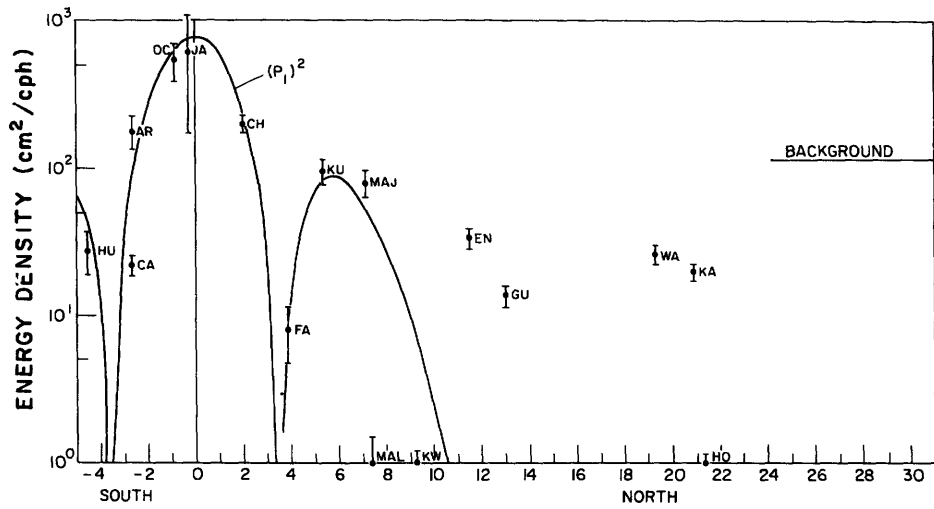
and

$$\frac{\partial \phi}{\partial \eta} = 0 \qquad \text{at} \quad z = -ax \tag{10.95}$$

plus boundedness of the velocity field ($\partial \phi/\partial x, ik\phi$, $\partial \phi/\partial z$) as $x \to \infty$. He found (1) a finite number of coastally trapped modes with dispersion relation
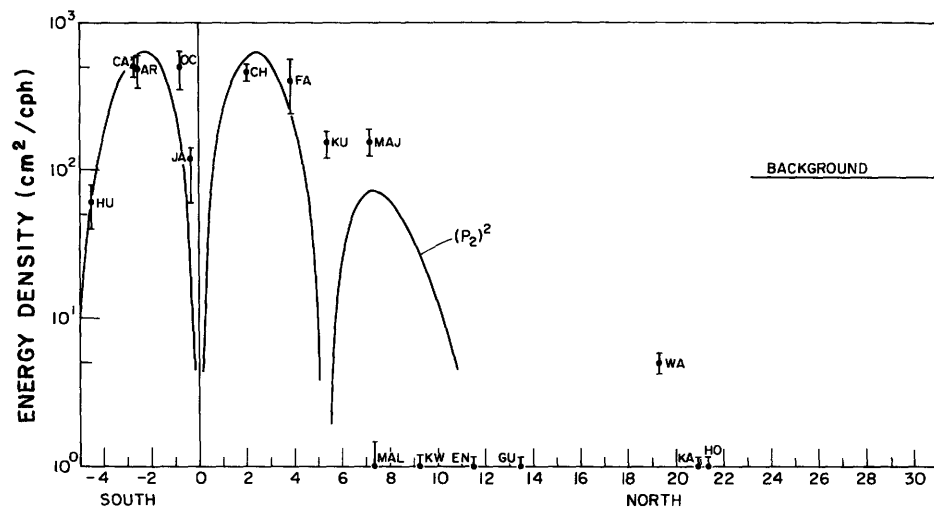
$$\sigma^2 = kg\sin[(2n + 1)\tan^{-1}a], \tag{10.96}$$
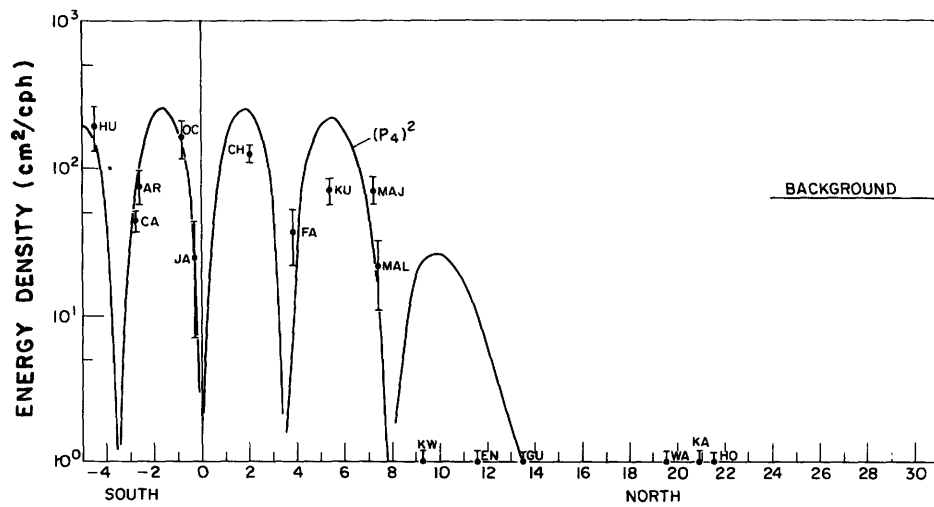$$n = 0, 1, \ldots < [\pi/(4\tan^{-1}a)^{-1/2}]$$

(10.11A)

(10.11B)

(10.11C)

Figure 10.11 Energy at periods of 5.6d, $m = 1$ (A); 4.0d, $m = 2$ (B); 3.0d, $m = 4$ (C); in tropical Pacific sea-level records as a function of latitude. A constant (labeled BACKGROUND) representing the background continuum has been subtracted from each value. Error bars are one standard deviation of χ^2. The solid curves are the theoretical latitudinal structure from the equatorial β-plane. (Wunsch and Gill, 1976.)

308
Myrl C. Hendershott

corresponding, for low n, to Eckart's results, plus (2) a continuum of solutions corresponding to the coastal reflection of deep-water waves incident from $x = \infty$ and correspondingly not coastally trapped. Far from the coast, the continuum solutions have the form $\phi = \cos(lx + \text{phase}) \exp[-i\sigma t + iky + (l^2 + k^2)^{1/2}z]$ and their dispersion relation must require $\sigma^2 \geq gk$. They are filtered out by the shallow-water approximation. Figure 10.12 compares Eckart's (1951) and Ursell's (1952) dispersion relations.

With rotation f_0 restored to (10.18), (10.90) becomes (Reid, 1958)

$$x\frac{\partial^2 h}{\partial x^2} + \frac{\partial h}{\partial x} + \left[\left(\frac{\sigma^2 - f_0^2}{ag} - \frac{f_0 k}{\sigma}\right) - xk^2\right]h = 0. \quad (10.97)$$

Solutions still have the form (10.89), (10.92) but now the dispersion relation is

$$\sigma^2 - f_0^2 - f_0 kag/\sigma = k(2n + 1)ag, \quad (10.98)$$

which is cubic in σ, whereas with $f_0 = 0$ it was quadratic. Rotation has evidently introduced a new class of motion.

That this should be so is clear from the β-plane vorticity equation [obtained by cross-differentiating (10.30a,b) and with $\partial f_0/\partial y = \beta$]:

$$\frac{\partial}{\partial t}\left(\frac{\partial v}{\partial x} - \frac{\partial u}{\partial y}\right) - \frac{f_0}{D}\frac{\partial \zeta}{\partial t} - u\frac{f_0}{D}\frac{\partial D}{\partial x} - v\left(-\beta + \frac{f_0}{D}\frac{\partial D}{\partial y}\right)$$

$$=0. \quad (10.99)$$

We have already seen (section 10.4.4) that the term βv gives rise to short and long Rossby waves (with the vortex-stretching term $f_0/D\ \partial\zeta/\partial t$ important only for the latter) when the depth is constant. But in (10.99), the topographic vortex-stretching term $uf_0/D\cdot\nabla D$ plays a role entirely equivalent to that of $\beta v = \mathbf{u}\cdot\nabla f_0$. Hence, we expect it to give rise to second-class waves, both short and long, even if $\beta = 0$. Such waves are called *topographic Rossby waves*. Over the linear beach $D = -ax$ they are all refractively trapped near the coast.

The nondimensionalization

$$s = \sigma/f, \quad K = kag/f^2 \quad (10.100)$$

casts the dispersion relation into the form

$$s^3 - s[1 + (2n + 1)K] - K = 0, \quad (10.101)$$

which is remarkably similar to (10.82) and plotted in figure 10.13.

The linear beach $D = ax$ is most unreal in that there is no deep sea of finite depth in which LSW plane waves can propagate. When the relief is modified to

$$D(x) = \begin{cases} ax, & 0 < x < D_0 a^{-1} & (\text{shelf}) \\ D_0, & D_0 a^{-1} < x < \infty & (\text{sea}), \end{cases} \quad (10.102)$$
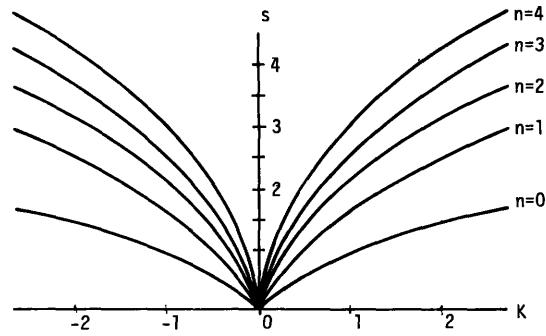

Figure 10.12A Eckart's (1951) dispersion relation (10.91)

$$s^2 = K(2n + 1)$$

for the shallow-water waves over a semi-infinite uniformly sloping, nonrotating beach. For convenience in plotting, $s = \sigma/f$ and $K = gak/f^2$ even though problem is not rotating.
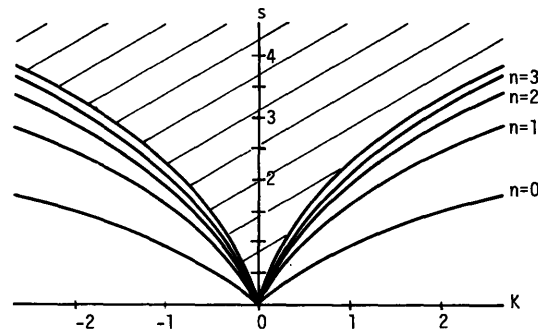

Figure 10.12B Ursell's (1952) dispersion relation (10.96)

$$s^2 = Ka^{-1}\sin[(2n + 1)\tan^{-1}a]$$

for edge waves, and the continuum

$$s^2 > Ka^{-1}$$

of deep-water reflected waves. For convenience in plotting, s and K are defined as above. Plot is for $a = 0.2$.
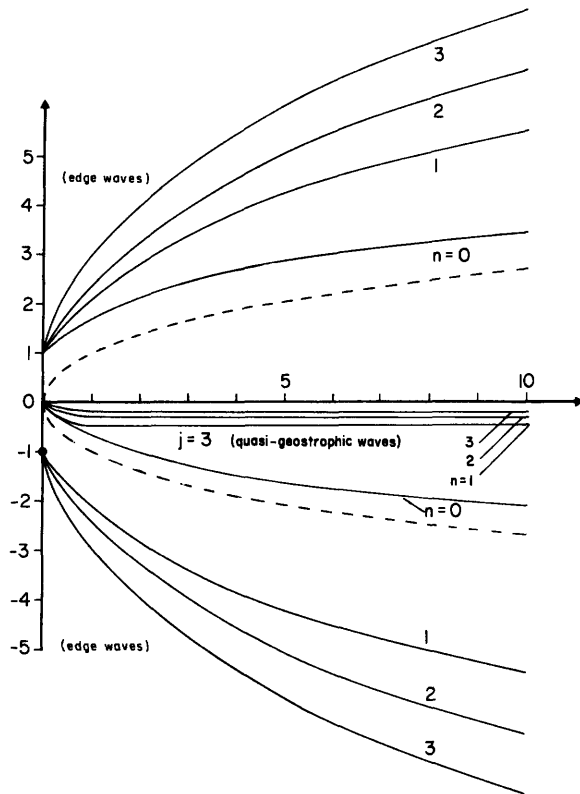
Figure 10.13 The dispersion relation (10.91) for edge and quasi-geostrophic shallow-water waves over a semi-infinite uniformly sloping beach. The dashed curves are the Stokes solution without rotation [(10.91) with $n = 0$]. Axes are as in figure 10.12. (LeBlond and Mysak, 1977.)

the most important alteration of the dispersion relation is an "opening up" of the long-wavelength part of the dispersion relation to include a continuum analogous to that of Ursell (1952) but now consisting of LSW first-class waves incident from the deep sea and reflected back into it by the coast and shelf. These waves are not coastally trapped. They are often called *leaky modes* because they can radiate energy that is initially on the shelf out into the deep sea. There are no second-class counterparts because the deep sea with constant depth and $\beta = 0$ cannot support second-class waves.

The dispersion relation corresponding to (10.102) is plotted in figure 10.14. All of Eckart's modes are modified so that $\sigma^2 > f_0^2$ save one ($n = 0$, traveling with the coast to its right), which persists as $\sigma \to 0$ and is a Kelvin-like mode. The others cease to be refractively trapped at superinertial ($>f_0$) individual cutoff frequencies bordering the continuum of leaky modes. At subinertial frequencies there is an infinite family of refractively trapped topographic Rossby waves, all traveling with the coast to their right (like the Kelvin mode) and all tending toward the constant frequency $s = -1/(2n + 1)$ at small wavelengths. This dispersion relation is qualitatively correct for most other shelf

shapes. It differs from its equatorial β-plane counterpart (10.82) only in the absence of a mixed Rossby-gravity (Yanai) mode and in the tendency of short second-class modes to approach constant frequencies.

Topographic vortex stretching plus refraction of both first- and second-class waves are effective over any relief. Thus islands with beaches, submerged plateaus, and seamounts can in principal trap both first- and second-class barotropic waves (although these topographic features may have to be unrealistically large for their circumference to span one or more wavelengths of a trapped first-class wave). A submarine escarpment can trap second-class waves (then called *double Kelvin waves*; Longuet-Higgins, 1968b). Examples of such solutions are summarized by Longuet-Higgins (1969b) and by Rhines (1969b).

First-class waves trapped over the Southern California continental shelf have been clearly observed by Munk, Snodgrass, and Gilbert (1964), who computed the dispersion relation for the actual shelf profile and found (figure 10.15) sea-level variation to be closely confined to the dispersion curves thus predicted for periods of order of an hour or less. Both first- and second-class coastally trapped waves may be variously significant in coastal tides [Munk, Snodgrass, and Wimbush (1970) and section 10.5.2]. At longer periods, a number of observers claim to have detected coastally trapped second-class modes (Leblond and Mysak, 1977). A typical set of observations is shown in figure 10.16, after R. L. Smith (1978).

10.4.7 Long Waves over Relief with Rotation and Stratification

The two mechanisms of refraction and vortex stretching that govern the behavior of long waves propagating in homogeneous rotating fluid over bottom relief are sufficiently well understood that qualitatively correct dispersion relations may be found intuitively for quite complex relief even though their quantitative construction might be very involved. Stratification complicates the picture greatly. In this section, emphasis is upon problems with stratification that may be solved with sufficient completeness that they augment our intuition.

By appealing to the quasi-geostrophic approximation, Rhines (1975; 1977) has given a far-reaching treatment of the interplay between beta, weak bottom slope, and stratification for second-class waves. If equations (10.30a) and (10.30b) are cross-differentiated to eliminate pressure, and continuity (10.30d) is then invoked, the result is

$$\frac{\partial}{\partial t}\left(\frac{\partial v}{\partial x} - \frac{\partial u}{\partial y}\right) + \beta v - f_0 \frac{\partial w}{\partial z} = 0$$

in the β-plane approximation (section 10.4.4) $f = f_0$, $\beta = \partial f/\partial y$. Now this equation is recast as an approxi-
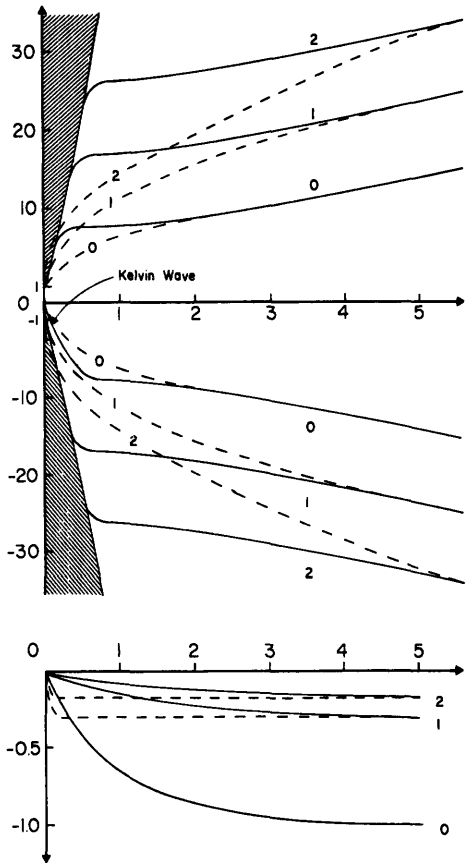
Myrl C. Hendershott

Figure 10.14 The dispersion relation (solid lines) for edge and quasi-geostrophic shallow-water waves over a uniformly sloping beach (slope $a = 2 \times 10^{-3}$) terminating in a flat ocean floor at a depth of $D = 5000$ m. The dotted lines are for the semi-infinite uniformly sloping beach. The shaded region is the continuum of leaky modes. Axes are as in figure 10.12. (Leblond and Mysak, 1977.)

mate equation in p by using (10.30c) plus the geostrophic approximation to obtain

$$\frac{\partial}{\partial t}\left(\frac{\partial^2 p}{\partial x^2} + \frac{\partial^2 p}{\partial y^2} + \frac{f_0^2}{N_0^2}\frac{\partial^2 p}{\partial z^2}\right) + \beta\frac{\partial p}{\partial x} = 0. \qquad (10.103)$$

This result emerges from a more systematic treatment (Pedlosky, 1964a) as the linearized quasi-geostrophic approximation. It is here specialized to the case of constant buoyancy frequency N_0. The free surface may be idealized as rigid without loss of generality; the corresponding condition on p is

$$\frac{\partial p}{\partial z} = 0 \qquad \text{at} \quad z = 0. \qquad (10.104)$$

The inviscid bottom boundary condition $w = av$ at the north–south sloping bottom $z = -D_0 + ay$ becomes, in quasi-geostrophic approximation,

$$-\frac{\partial^2 p}{\partial t\,\partial z} + a\frac{N_0^2}{f_0}\frac{\partial p}{\partial x} = 0 \qquad \text{at} \quad z = -D_0, \qquad (10.105)$$

and is linearized about $z = -D_0$ for sufficiently small a.

With no bottom slope, solutions of (10.103)–(10.105) are

$$P = \cos(\lambda z)\exp(-i\sigma t + ilx + iky), \qquad (10.106)$$

$$\sigma = -\beta l/(l^2 + k^2 + \lambda^2 f_0^2/N_0^2), \qquad (10.107)$$

with λ given by (10.105) as a solution of

$$\sin(\lambda D_0) = 0 \qquad (10.108)$$

i.e.,

$$\lambda = n\pi/D_0, \qquad n = 0, 1, 2, \ldots \qquad (10.109)$$

These correspond to the barotropic $(n = 0)$ and baroclinic $(n = 1, 2, \ldots)$ Rossby waves of section 10.4.4.

With no beta but with bottom slope, solutions of (10.103)–(10.105) are

$$P = \cosh(\lambda z)\exp(-i\sigma t + ilx + iky), \qquad (10.110)$$

$$\lambda = (N_0/f_0)(l^2 + k^2)^{1/2}, \qquad (10.111)$$

$$\sigma = \frac{aN_0^2\coth(\lambda D_0)}{\lambda f_0}. \qquad (10.112)$$

If $\lambda D_0 \ll 1$, p is virtually depth independent and the dispersion relation (10.112) becomes

$$\sigma = D_0^{-1}af_0l/(l^2 + k^2). \qquad (10.113)$$

This is a barotropic topographic Rossby wave with vortex stretching over the relief playing the role of beta. If $\lambda D_0 \gg 1$, p decays rapidly away from the bottom and the dispersion relation (10.112) becomes

$$\sigma = N_0l/(l^2 + k^2)^{1/2}. \qquad (10.114)$$

Such *bottom-trapped* motions are of theoretical importance because they allow mid-latitude quasi-geostrophic vertical shear and density perturbations at periods much shorter than the very long ones predicted by the flat-bottom baroclinic solutions (10.106)–(10.109). Rhines (1970) generalizes this bottom-trapped solution to relief of finite slope and points out that it reduces to the usual baroclinic Kelvin wave at a vertical boundary. Figure 10.17 shows what appear to be motions of this type.

With both beta and bottom slope, solutions of (10.103) and (10.104) are

$$P = \frac{\cos}{\cosh}(\lambda z)\exp(-i\sigma t + ilx + iky) \qquad (10.115\substack{a\\b})$$

$$\sigma = -\beta l/(l^2 + k^2 \pm \lambda^2 f_0^2/N_0^2), \qquad (10.116\substack{a\\b})$$

with λ given by (10.105) as

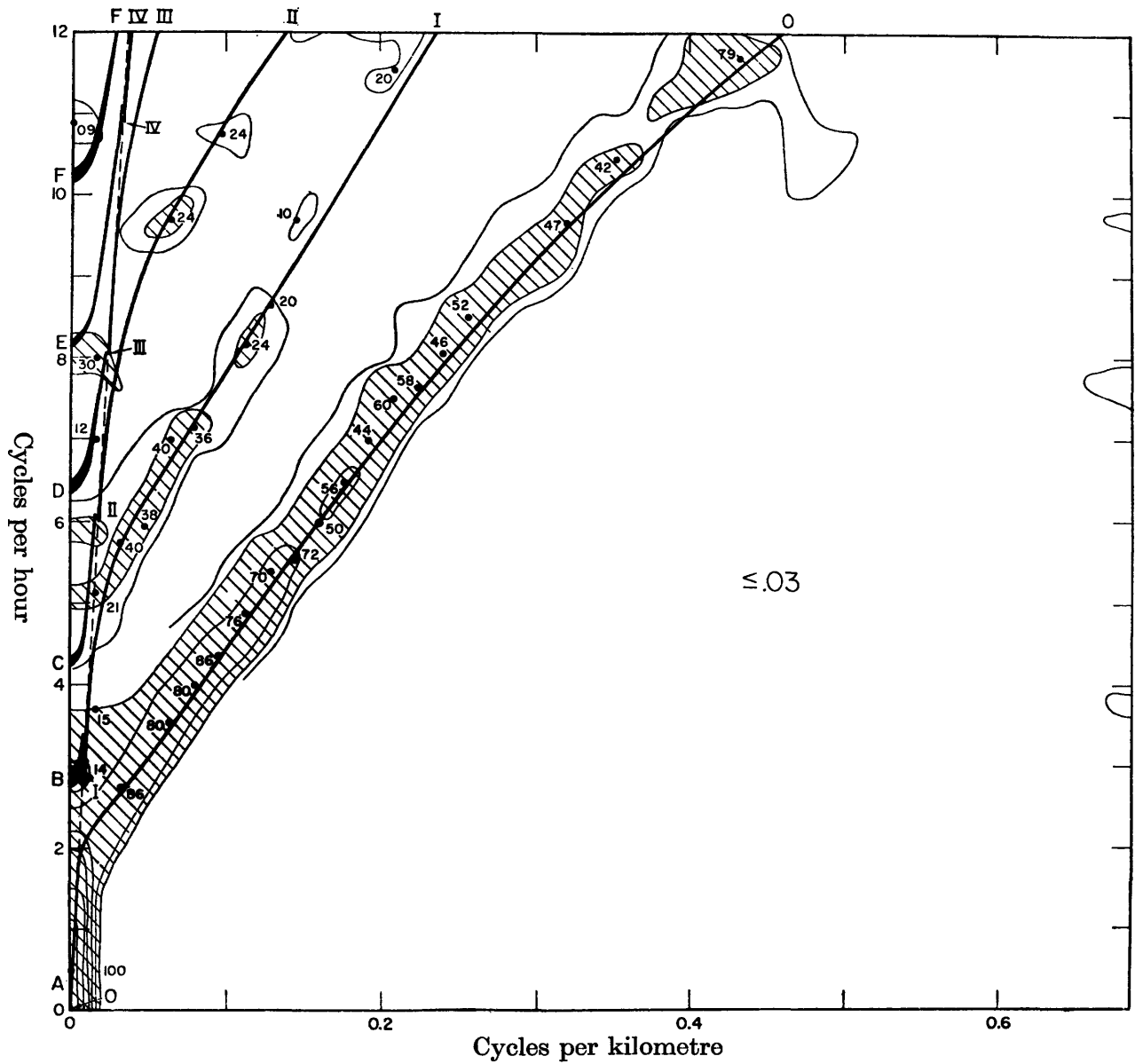$$\lambda\tan(\lambda D_0) = -\frac{aN_0^2}{f_0}\frac{l}{\sigma} \qquad (10.117a)$$

Figure 10.15 Comparison of theoretical and observed dispersion for the California continental shelf. Heavy lines 0-IV correspond to theoretical dispersion relations for the first five trapped first-class modes. The dashed line bounds the continuum of leaky modes. The observed normalized two-dimensional cospectrum of bottom pressure is contoured for values of 0.03, 0.05, 0.10, 0.25, 0.50, 0.75, and 0.90 with the area above 0.05 shaded. (Munk, Snodgrass, and Gilbert, 1964.)
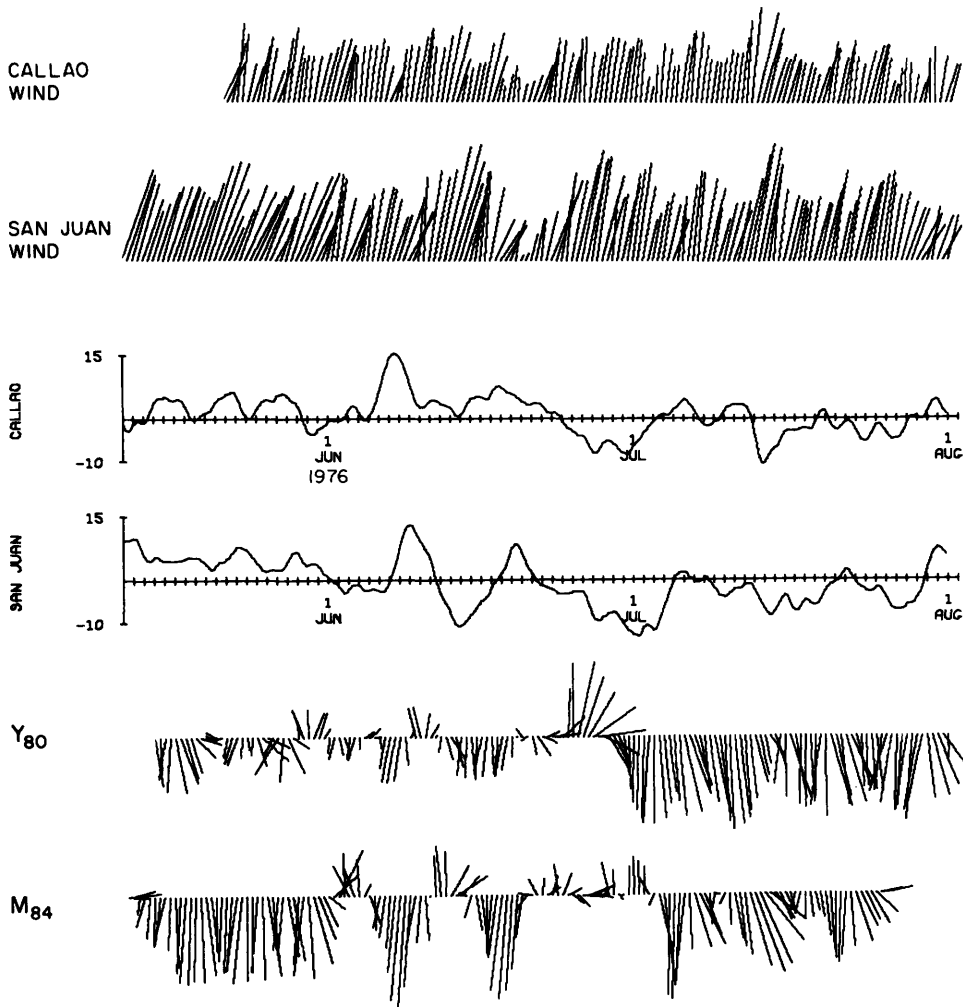
Myrl C. Hendershott

Figure 10.16 Low-passed wind vectors and sea-level records from Callao (12°04′ S) and San Juan (15°20′ S), Peru, and current vectors from Y (80 m below surface off Callao) and from M (84 m below surface off San Juan). Sea level and currents show propagation of events along the coast; wind records do not. (R. L. Smith, 1978.)

for case (a) and

$$\lambda \tanh(\lambda D_0) = \frac{aN_0^2}{f_0}\frac{1}{\sigma} \qquad (10.117b)$$

for case (b). Equation (10.117b) has one root λ corresponding to a bottom-trapped wave for large a and to a barotropic β-wave for vanishing a. For vanishing a, (10.117a) reproduces the familiar flat-bottom barotropic and low-frequency baroclinic modes $\lambda = n\pi/D_0$, $n = 0, 1, \ldots$. When a is large the baroclinic roots are shifted toward $\lambda \simeq (\pi/2 + n\pi)/D_0$, so that the pressure (10.115a) and hence the horizontal velocity have a node at the bottom. There is thus a tendency for relief to result in the concentration of low-frequency baroclinic energy away from the bottom. With more realistic stratification this concentration is increasingly in the upper ocean. Rhines (1977) therefore calls such motions "thermocline eddies" and suggests that they are relevant to the interpretation of the observations of figure 10.18. It is straightforward to allow for an arbi-

trary direction of the bottom slope, but the results are not easy to summarize. Rhines (1970) gives a complete discussion.

A powerful treatment of second-class motion in a rotating stratified fluid over the linear beach $D = ax$ has been provided by Ou (1979), Ou (1980), and Ou and Beardsley (1980). They have generously permitted me to make use of their results in this discussion. Neglecting free surface displacement (so that $w = 0$ at $z = 0$) and eliminating u,v,w from (10.30) in favor of p yields

$$\frac{\partial^2 p}{\partial z^2} + \frac{N^2}{f_0^2 - \sigma^2}\left(\frac{\partial^2 p}{\partial x^2} + \frac{\partial^2 p}{\partial y^2}\right) = 0, \qquad (10.118)$$

$$\frac{\partial p}{\partial z} = 0 \quad \text{at} \quad z = 0, \qquad (10.119)$$

$$a\left(i\sigma\frac{\partial p}{\partial x} - f_0\frac{\partial p}{\partial y}\right) + i\sigma\frac{f_0^2 - \sigma^2}{N_0^2}\frac{\partial p}{\partial z} = 0 \qquad (10.120)$$
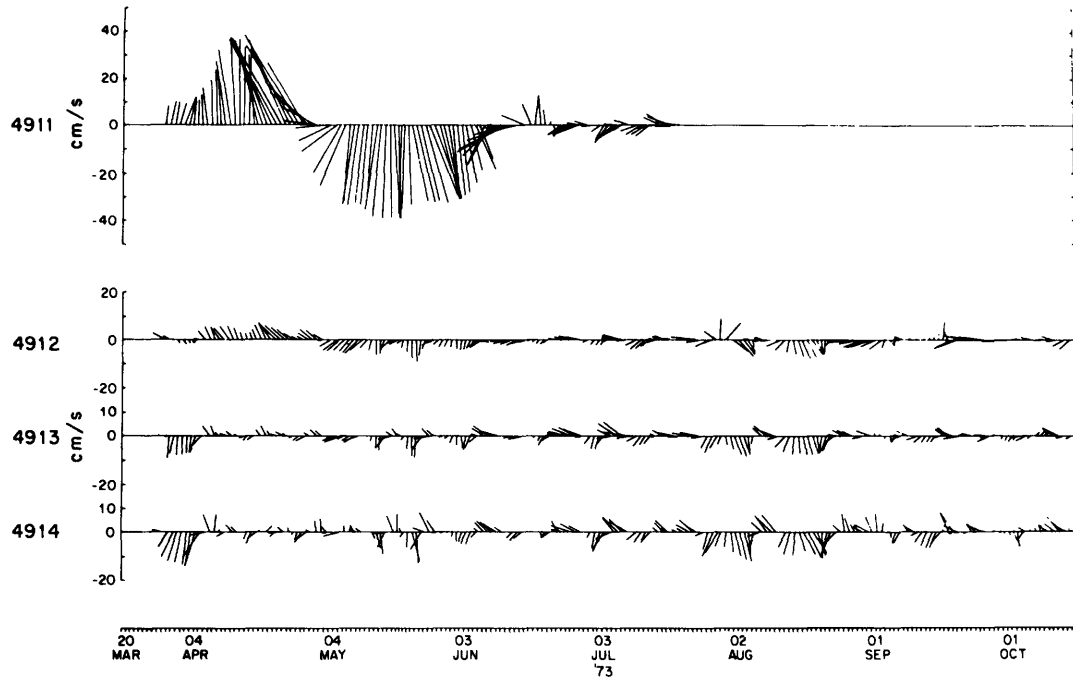
at $z = -ax$

Figure 10.17A Currents at 39°10′N, 70°W (site D) at 205, 1019, 2030, and 2550 m. The total depth is 2650 m. A "thermocline" eddy initially dominates the upper flow.
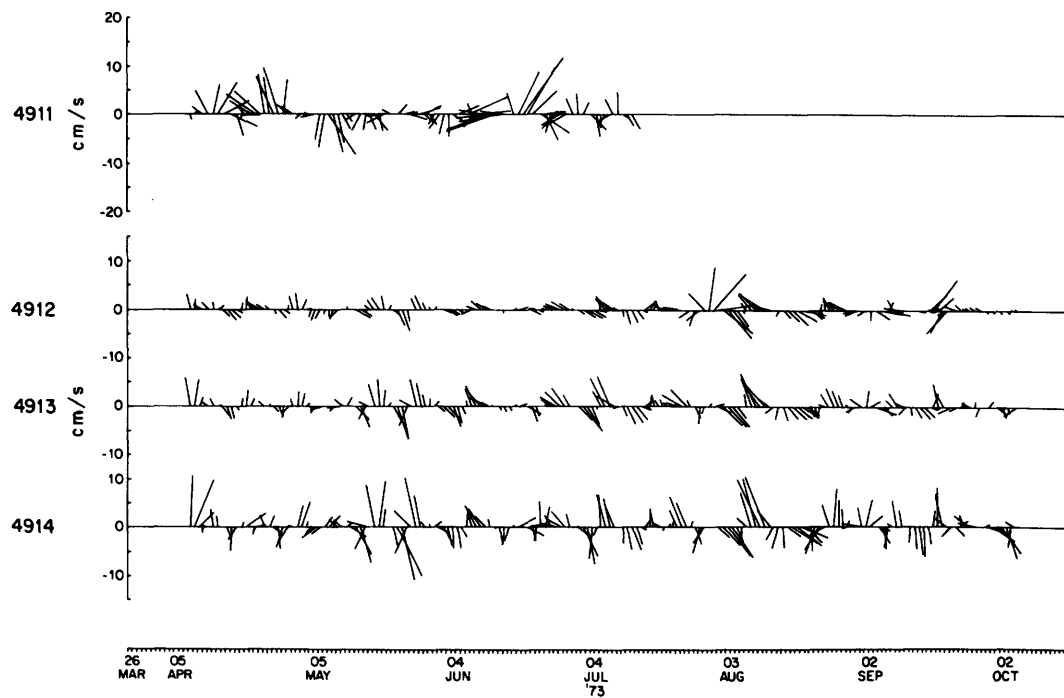

Figure 10.17B A high-passed version of figure 10.17A. The lower layers are now dominated by fast-bottom intensified oscillations. (Rhines, 1977.)
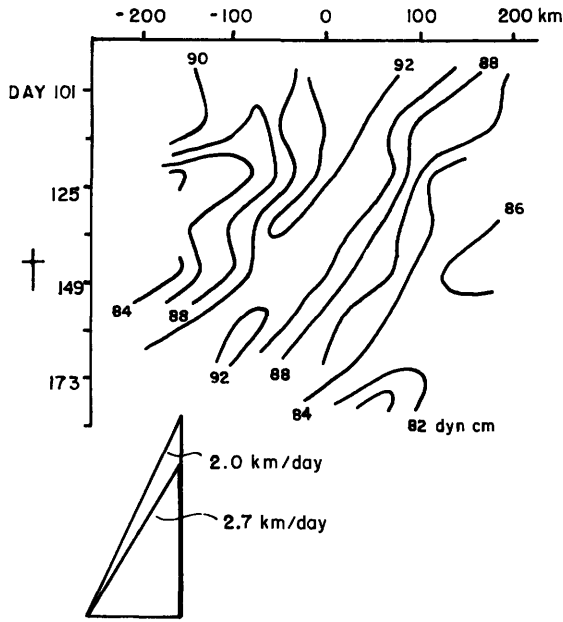
314
Myrl C. Hendershott

Figure 10.18 Time–longitude plot of 501–1500-db dynamic height along 28′N from MODE showing westward propagation of "thermocline eddies" but at a rate significantly slower than that observed in 1500-m currents (figure 10.6). (Rhines, 1977.)

as the boundary-value problem governing periodic [exp($-i\sigma t$)] second-class (and low-frequency first-class internal) waves over the linear beach. Ou (1979) saw that the affine transformation

$$\hat{z} = \hat{z}(f_0^2 - \sigma^2)^{1/2}/N_0 \qquad (10.121)$$

followed by a rotation of coordinates from $(x, y, \hat{z})$ to (x', y, z') such that the beach $z = -ax$ now becomes $z' = 0$ leads to

$$\frac{\partial^2 p}{\partial z'^2} + \frac{\partial^2 p}{\partial x'^2} - k^2 p = 0, \qquad (10.122)$$

$$\frac{\partial p}{\partial n} = \frac{kf_0}{\sigma} \frac{a'}{(1 + a'^2)^{1/2}} p \quad \text{at} \quad z' = 0, \qquad (10.123)$$

$$\frac{\partial p}{\partial n} = 0 \quad \text{at} \quad z' = a'x' \qquad (10.124)$$

for motions periodic in y [exp(iky)], and furthermore that this is *exactly* Ursell's (1952) problem just turned upside down; (10.122), (10.123), and (10.124) correspond to (10.93), (10.94), and (10.97). The transformed beach slope a' is given by

$$a' = aN(f_0^2 - \sigma^2)^{-1/2}. \qquad (10.125)$$

For second-class waves

$$\sigma^2 < f_0^2, \qquad (10.126)$$

a' is real and all of Ursell's (1952) results are immediately available. There are thus coastally trapped waves whose dispersion relation is

$$\sigma = f_0 a'/\{(1 + a'^2)^{1/2} \sin[(2n + 1)\tan^{-1}a']\} \qquad (10.127)$$

as well as a continuum of bottom-trapped waves that have the form

$$P = \cos(lx' + \text{phase}) \exp[-i\sigma t + iky - (l^2 + k^2)^{1/2}z']$$

as $x' \to \infty$ and that have their dispersion relation included in

$$\sigma = -N \sin(\tan^{-1}a) \left[\frac{k}{(l^2 + k^2)^{1/2}} \right]. \qquad (10.128)$$

The latter are just the bottom-trapped waves (10.110)–(10.112) of Rhines (1970).

Equation (10.128) is their dispersion relation in a half-plane bounded by the sloping bottom (Rhines, 1970). The frequency may be either sub- or super-inertial. The coastally trapped waves have $\sigma > N \sin(\tan^{-1}a)$ [by analogy with the fact that for Ursell's (1952) edge waves $\sigma^2 < gk$] and there are a finite number of them:

$$n = 1, 2, \ldots < [\pi/(4\tan^{-1}a') - 1/2]. \qquad (10.129)$$

Note that $n = 0$ would imply $\sigma = f_0$ but this does not solve the full equations (10.30) and associated boundary conditions.

In the limit of decreasing slope a', (10.129) allows ever more modes, and the dispersion relation (10.127) for coastally trapped waves simplifies to

$$\sigma = -f_0(2n + 1). \qquad (10.130)$$

This is the low-frequency, short-wavelength second-class limit of the barotropic dispersion relation (10.98). We thus identify Ou's coastally trapped modes as the stratified analog of the already familiar refractively trapped second-class topographic Rossby waves.

Over the linear beach, then, stratification limits the number of second-class refractively trapped topographic waves and opens up a new continuum of bottom-trapped waves. Figure 10.19 compares barotropic and baroclinic dispersion relations when the ocean surface is rigid. Further results are given by Ou (1979).

Suppose now that the linear beach terminates in a flat bottom of depth D_0, as in (10.102). Ou's (1979) transformation allows us to deal efficiently with the stratified problem. Figure 10.20 summarizes the boundary-value problem and its alteration by Ou's transformation into an equivalent problem in deep-water waves (figure 10.20D). In this latter problem, the deep-water continuum that existed for the linear beach must now be quantized into an infinite family of modes by repeated reflection between the shoaling and the
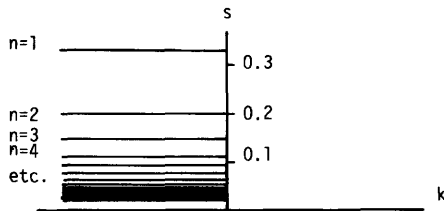
Figure 10.19A The dispersion relation (10.130), viz., $s = -1/(2n + 1)$ for topographic Rossby waves refractively trapped over the linear beach $D = -ax$ beneath rotating homogeneous fluid. There are an infinite number $n = 1,2,...$ of trapped modes.
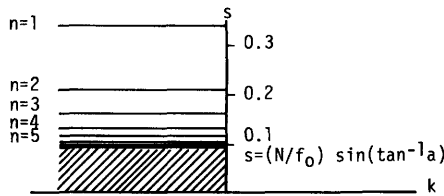

Figure 10.19B The dispersion relation (10.127)

$$s = a'/\{(1 + a'^2)^{1/2} \sin[(2n + 1)\tan^{-1}a']\},$$

where $a' = aN_0/[f_0(1 - s^2)^{1/2}]$, for topographic Rossby waves refractively trapped over the linear beach $D = -ax$ beneath uniformly stratified (buoyancy frequency N_0) rotating fluid. There are a finite number $n = 1,2,... < [\pi/(4\tan^{-1}a') - \frac{1}{2}]$ of trapped modes all with frequencies $s > N_0 f_0^{-1} \sin[\tan^{-1}a]$. At lower frequencies a continuum of bottom-trapped modes reflected from $x = \infty$ exists. Sketch is for $N_0 = 10 f_0$, $a = 10^{-2}$.
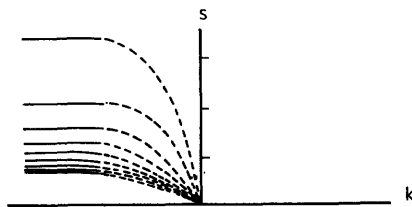

Figure 10.19C Sketch of dispersion relation for topographic Rossby waves in rotating stratified fluid over a linear beach that terminates in a uniform-depth ocean. The continuum of bottom-trapped modes that existed over the semi-infinite beach is quantized. All dispersion curves pass through $s = 0$ as $k \to 0$.

overhanging coasts. Low-mode edge waves have small amplitude at the overhanging coast and are not much affected by it. But higher-mode edge waves have appreciable amplitude at the overhanging coast and they blend smoothly into the infinite family of modes made up of waves repeatedly reflected between beach and the overhanging coast. All these results have direct analogs in the original stratified problem (figure 10.20A). There are a number of second-class topographic waves that are refractively trapped near the coast and that have decayed to very small amplitudes at the seaward termination of the beach. The continuum of bottom-trapped waves present over the unending linear beach is replaced by an infinite family of bottom-trapped waves reflected repeatedly between the coast and the seaward termination of the beach. In the special case $a = \infty$ of a perpendicular coast, their dispersion relations are easily seen to be

$$\sigma = ND_0 k/n\pi \tag{10.131}$$

and they then correspond to ordinary internal Kelvin waves (in this case there are no refractively trapped modes). Other shelf geometries invite similar treatment. Figures 10.20E and 10.20F show the equivalent deep-water wave problem for a step shelf. Deep-water waves on surface 1 of figure 10.20F that are short enough that their particle displacements at the level of surface 2 are negligible correspond in the stratified problem (figure 10.20E) to internal Kelvin waves trapped against the coast. Deep-water waves on surface 2 of figure 10.20F correspond to baroclinic counterparts of the double Kelvin wave that, in homogeneous fluid, may be trapped along a discontinuity in depth (Longuet-Higgins, 1968b; see also section 10.4.6).

In general, if the equivalent deep-water wave problem has the waveguide-like dispersion relations $\sigma^2/g = F_n(H, \gamma, k)$, $n = 1, 2, \ldots$, with H, γ as defined in figure 10.20D, then the corresponding stratified shelf problem must have the dispersion relation

$$\frac{kf}{\sigma} - \frac{a'}{(1 + a'^2)^{1/2}} = F_n[((D_0 a'/a)^2 + D_0 a^{-2})^{1/2},$$

$$\tan^{-1}a', k] \tag{10.132}$$

so that for all the dispersion curves $\sigma \to 0$ as $k \to 0$. The dispersion relation must thus qualitatively look like figure 10.19C. Wang and Mooers (1976) have generalized the problem numerically to more complex shelf profiles with nonuniform stratification $N(z)$.

Ou's (1979) transformation is most useful for second-class motions (10.125) because for them the transformed coordinates are real. For first-class motions with $\sigma^2 > f_0^2$ it still produces Laplace's equation but now z' is imaginary. Wunsch (1969) has nonetheless been able to use it to discuss first-class internal waves obliquely incident on the linear beach without rota-
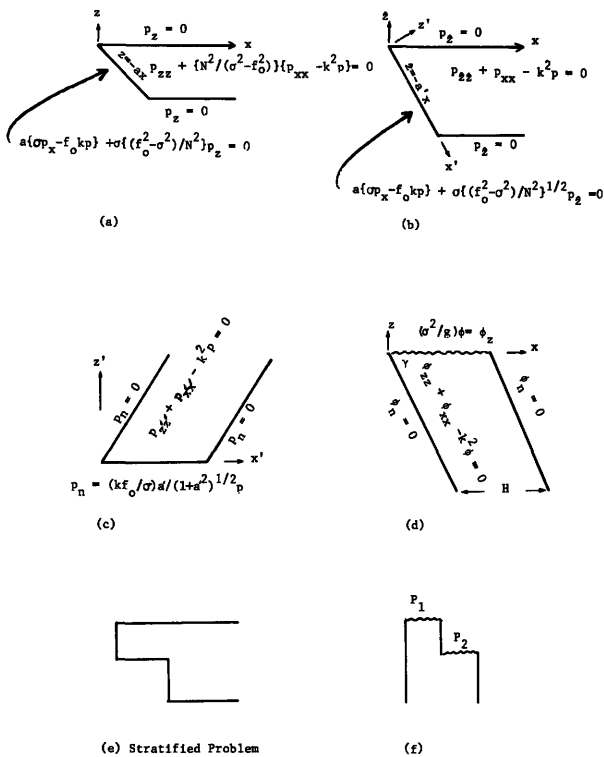
Myrl C. Hendershott

Figure 10.20 The deep-water surface-wave analog (d,f) of two shelf problems involving topographic Rossby waves in uniformly stratified rotating fluid: (a) stratified problem; (b) result of affine transformation; (c) result of rotation; (d) equivalent deep-water problem (velocity potential ϕ); (e) stratified problem; (f) equivalent deep-water problem (atmospheric pressure P_1 must be maintained lower than P_2 for physical realizability).

tion. This is the stratified analog of Eckart's (1951) nonrotating LSW study of waves over a sloping beach (section 10.4.6).

For beach slopes much smaller than the slope (σ/N) of (low-frequency) internal wave characteristics (10.43), Wunsch thus found that internal waves are refracted just like surface gravity waves by the shoaling relief and that refractively trapped edge modes occur. From the dispersion relation

$$\left(\frac{n\pi}{D_0}\right)^2 = \frac{N^2 - \sigma^2}{\sigma^2}\,(l^2 + k^2)$$

for plane internal waves of the form

$$w = \sin\left(\frac{n\pi z}{D_0}\right)\exp(-i\sigma t + ilx + iky)$$

over a uniform bottom D_0, l must ultimately become imaginary if D_0 is allowed to grow parametrically offshore while n and k are held fixed. One would therefore expect a WKB treatment of internal waves over gently shoaling relief to result in refraction and refractive trapping *provided* that the mode number n does not

change, i.e., provided that the relief does not scatter energy from one mode into others. Constancy of n is indeed a feature of Wunsch's solutions but it cannot be expected to hold for more abrupt relief, especially if the relief slope exceeds the characteristic slope. If the relief couples modes efficiently, then scattering into higher modes allows l to remain real even in deep water far from shore so that energy is not refractively trapped near the coast. In principle, scattering into internal modes thus even destroys the perfect trapping of long surface gravity waves predicted by LSW theory over a step shelf, but in practice appreciable trapping is often observed. The efficiency of mode coupling depends both on the relief and on the vertical profile $N(z)$ of the buoyancy frequency, so that a general result for internal waves is difficult to formulate.

10.4.8 Free Oscillations of Ocean Basins
Finding the free oscillations allowed by LTE in rotating ocean basins is difficult even in the f-plane (section 10.4.2). Platzman (1975, 1978) has developed powerful numerical techniques for finding the natural frequencies and associated flow fields of free oscillations allowed by LTE in basins of realistic shape and bottom relief. The general classification of free oscillations into first- and second-class modes characteristic of the idealized cases discussed in sections 10.4.2 and 10.4.5 (effectively for a global basin) persists in Platzman's (1975) calculations. For a basin composed of Atlantic and Indian Oceans, there are 14 free oscillations with periods between 10 and 25 hours. Some of these are very close to the diurnal and semidiurnal tidal periods, and all of them, being within a few percentage points of equipartition of kinetic and potential energies, are first-class modes. There are also free oscillations of much longer period, for which potential energy is only about 10% or even less of kinetic energy; they are second-class modes.

I know of no extratidal peaks in open-ocean sea-level records that correspond to these free oscillations. There is some evidence in tidal admittances for the excitation of free modes but the resonances are evidently not very sharp (see section 10.5.1). Munk, Bryan, and Zetler (private communication) have searched without success for the intertidal coherence of sea level across the Atlantic that the broad spatial scale of these modes implies. The modes are evidently very highly damped.

10.5 The Ocean Surface Tide

10.5.1 Why Ocean Tides Are of Scientific Interest
The physical motivation for studying and augmenting the global ensemble of ocean-tide records has expanded enormously since Laplace's time. In this section I have tried to sketch the motivating ideas without getting